UNIVERSIDADE
BEIRA INTERIOR

Development of polymer-gold nanohybrids for the combinatorial therapy of cancer

André Filipe Quelhas Figueiredo

Dissertação para obtenção do Grau de Mestre em
Bioquímica
(2º ciclo de estudos)

Orientador: Prof. Doutor Ilídio Joaquim Sobreira Correia
Co-orientador: Doutor André Ferreira Moreira
Co-orientador: Mestre Ana Carolina Félix Rodrigues

outubro de 2022

Declaração de Integridade

Eu, André Filipe Quelhas Figueiredo, que abaixo assino, estudante com o número de inscrição M11036 de Bioquímica da Faculdade de Ciências, declaro ter desenvolvido o presente trabalho e elaborado o presente texto em total consonância com o **Código de Integridades da Universidade da Beira Interior**.

Mais concretamente afirmo não ter incorrido em qualquer das variedades de Fraude Académica, e que aqui declaro conhecer, que em particular atendi à exigida referenciação de frases, extratos, imagens e outras formas de trabalho intelectual, e assumindo assim na íntegra as responsabilidades da autoria.

Universidade da Beira Interior, Covilhã, 6 / 10 / 2022

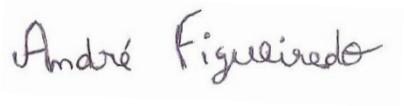

(assinatura conforme Cartão de Cidadão ou preferencialmente
assinatura digital no documento original se naquele mesmo formato)

“Education is the most powerful weapon which you can use to change the world”

Nelson Mandela

Dedication

Dedico este trabalho à minha família, pais, irmão, avós e à Rita pelo apoio constante e pelas palavras de incentivo que me encorajaram para enfrentar com um sorriso todo o meu percurso académico.

Acknowledgments

Em primeiro lugar, quero agradecer ao meu orientador Professor Doutor Ilídio Correia, pela oportunidade de ter pertencido ao seu grupo de investigação e por me ter disponibilizado todas as condições para que eu pudesse desenvolver este trabalho de investigação. Agradeço também a sua orientação rigorosa e com elevado valor científico, sem nunca deixar de parte a boa disposição e o bom ambiente em ambiente laboral, valores estes que me permitiram crescer muito em termos pessoais e profissionais.

Ao meu co-orientador, Doutor André Moreira, agradeço toda a ajuda, paciência e dedicação dadas ao longo desta dissertação, que nunca me deixaram desistir mesmo quando os obstáculos pareciam insuperáveis.

À minha co-orientadora Mestre Carolina Rodrigues, agradeço o esforço, a dedicação, o acompanhamento e o todos os ensinamentos que me deu este ano, facilitando mais esta etapa académica.

À Adriana, Francisco, Casa e Micaela pelos bons momentos passados neste ano e pelo companheirismo sempre demonstrado. Muito obrigado.

Ao restante grupo de investigação, em especial à Mariana, Bruna e Nata um obrigado pela ajuda e disponibilidade demonstrada ao longo deste ano.

A todos os amigos que levo desta universidade, em especial ao Patrik, amigo desde o primeiro dia que tornou estes anos académicos inesquecíveis (O 5ºesq. e o sumo de maça são eternos).

A todos os amigos da "terrinha" por serem amigos sempre presentes (apesar de ausentes fisicamente), muito obrigado.

À minha família, pelo apoio sempre prestável e por nunca deixaram que me faltasse nada nestes anos. Bem-haja!

Por fim quero agradecer à Rita por tudo, apoio incondicional, força e palavras encorajadoras que serviram de pilar para concretizar este obstáculo. Muito, muito obrigado.

Resumo

O cancro continua a ter um grande impacto na saúde pública mundial, com milhões de novos casos diagnosticados anualmente. Para além disso, esta doença tem uma elevada taxa de mortalidade associada devido às dificuldades de realizar um diagnóstico precoce, à sua rápida progressão e à falta de eficácia dos tratamentos convencionais, tais como a cirurgia, a quimioterapia e a radioterapia. De facto, o procedimento cirúrgico pode não assegurar a remoção completa do tumor e a radioterapia/quimioterapia apresentam uma baixa especificidade para as células cancerígenas, causando graves efeitos secundários. Por conseguinte, é urgente desenvolver e implementar novas abordagens terapêuticas que apresentem maior seletividade e eficácia.

Nos últimos anos, avanços na área da nanotecnologia têm permitido o desenvolvimento de novas soluções para melhorar o desempenho da eletrónica, do diagnóstico médico e da terapêutica. Particularmente, na terapia do cancro, as nanopartículas podem ser exploradas para desenvolver ferramentas de diagnóstico, imagiologia, agentes terapêuticos, permitindo ainda a combinação destas funções num único sistema multifuncional. Este potencial permitiu o desenvolvimento de diferentes nanopartículas, ao variar tanto a matéria-prima (por exemplo, polímeros, cerâmica, lípidos e materiais) como a estrutura das nanopartículas. Entre elas, as nanopartículas à base de metais, são dos materiais mais promissores para criar plataformas multifuncionais "tudo-em-um", devido à sua capacidade inerente para atuarem na imagiologia biológica, que pode ser combinada com a entrega de medicamentos ou efeitos fototermais/fotodinâmicos. No entanto, estes materiais apresentam frequentemente perfis de citotoxicidade e estabilidades coloidais desfavoráveis, bem como interações inespecíficas no corpo humano. Para abordar estas questões, as nanopartículas à base de metais têm sido frequentemente combinadas com outros materiais, tais como materiais inorgânicos (por exemplo, sílica) e/ou orgânicos (por exemplo, polímeros, como o Polietilenoglicol, PEG). Nesta área, a conjugação metal-polímero pode ser altamente vantajosa do ponto de vista biológico, nomeadamente através da melhoria da biocompatibilidade, estabilidade coloidal e especificidade tumoral.

Tomando isto em consideração, o plano de trabalhos desenvolvido durante esta dissertação teve como objetivo desenvolver uma nova metodologia de síntese de nanomateriais de ouro-ácido algínico para aplicação na terapia oncológica. O ouro é um dos materiais mais explorados para a produção de nanopartículas metálicas devido às

suas promissoras propriedades óticas (por exemplo, a ressonância plasmónica de superfície localizada), eficiência de conversão luz-calor, e fácil funcionalização. O ácido algínico foi selecionado devido à sua biocompatibilidade e hidrofilicidade, bem como a sua carga negativa, que foi explorada para orientar a formação dos nanomateriais. Para esse efeito, a produção dos nanomateriais foi conseguida promovendo a redução e nucleação do ouro na presença de ácido algínico e cloreto de cálcio. Os nanohíbridos de ouro-ácido algínico apresentaram uma morfologia similar a "estrelas", ou seja, com projeções na superfície, com o ouro reduzido disperso dentro da matriz das nanopartículas. Além disso, a redução do ouro *in situ* permitiu aumentar a absorção na região do NIR (infravermelho próximo), quando comparada com nanopartículas de ácido algínico, o que indicou o potencial de nanohíbridos de ouro-ácido algínico para aplicação na terapia fototérmica. Adicionalmente, os ensaios de estabilidade coloidal demonstraram que os nanohíbridos de ouro-ácido algínico permaneceram estáveis durante 3 semanas, sendo apenas detetada uma variação de tamanho de 4,7% depois de 21 dias. Por outro lado, os ensaios *in vitro* realizados em fibroblastos humanos (FibH) e células do cancro da mama (MCF-7) revelaram que os nanohíbridos de ouro-ácido algínico eram biocompatíveis, mesmo à concentração mais elevada testada de 200 μg mL^{-1}, após 72 h de incubação. Além disso, os ensaios de fluorescência demonstraram que as nanopartículas conseguem ser eficientemente internalizadas pelas células cancerígenas. Por fim, a irradiação com um laser de NIR (3 ciclos, 808 nm, 1,7 W cm^{-2} durante 10 min) resultou na redução da viabilidade das células MCF-7 para ≈27%, na presença de nanohíbridos de ouro-ácido algínico a uma concentração de 200 μg mL^{-1}.

Em suma, os resultados obtidos demonstram que a síntese de nanohíbridos de ouro-ácido algínico foi bem sucedida. Adicionalmente, foi demonstrada a estabilidade destes nanomateriais em solução, o seu potencial fototérmico, e a sua possível aplicação na terapia do cancro. No futuro, a funcionalização dos nanomateriais com agentes de direcionamento (por exemplo, anticorpos ou aptâmeros) e o encapsulamento de fármacos serão explorados para aumentar ainda mais a especificidade para o cancro por parte dos nanohíbridos de ouro-ácido algínico e subsequentemente permitir o desenvolvimento de terapias combinatórias quimiofotérmicas mais eficazes. Além disso, a realização de ensaios *in vivo* permitirá validar o potencial terapêutico dos nanohíbridos de ouro-ácido algínico.

Palavras-chave

Cancro; Nanomateriais; Nanopartículas de ouro; Ácido algínico; Terapia fototérmica

Resumo Alargado

Atualmente, o cancro continua a ser uma das doenças mais diagnosticadas e uma das principais causas de morte no mundo. Nas próximas décadas prevê-se que a incidência do cancro continue aumentar estando estes valores relacionados com o aumento da esperança média de vida da população mundial e a maior exposição a fatores de risco, como por exemplo a poluição ambiental. Por outro lado, as dificuldades em realizar um diagnóstico precoce, a rápida progressão da doença, e a falta de eficácia dos tratamentos convencionais são alguns dos fatores que contribuem para a elevada mortalidade do cancro. Os tratamentos convencionais, nomeadamente, a quimioterapia, cirurgia e radioterapia para além da baixa eficácia apresentam vários efeitos secundários associados. A quimioterapia e a radioterapia são principalmente afetadas pela baixa biodisponibilidade e especificidade para as células cancerígenas, induzindo frequentemente graves efeitos secundários em células saudáveis. Relativamente aos procedimentos cirúrgicos, estes não garantem a completa remoção de toda a massa cancerígena, devido à complexidade do tecido tumoral e da própria operação. Desta forma, os investigadores têm sido impulsionados a suprir a necessidade de se desenvolver novas abordagens terapêuticas que apresentem uma maior eficácia no tratamento do cancro. Nos últimos anos, avanços na área da nanotecnologia tem permitido o desenvolvimento de diferentes nanopartículas, baseadas em materiais como polímeros, lípidos ou metais, que oferecem novas soluções para melhorar o desempenho e a eficácia em diversas áreas, como a eletrónica, o diagnóstico médico e a terapêutica. Na terapia anti-cancerígena, as nanopartículas têm sido exploradascomo agentes de diagnóstico, imagiologia e/ou terapia (p.ex., entrega de fármacos). Esta utilização é suportada pela capacidade intrínseca das nanopartículas se acumularem no tecido tumoral, o que resulta num aumento da especificidade e diminuição dos efeitos secundários. Entre os diferentes tipos de nanopartículas que têm sido exploradas, as produzidas utilizando metais são das mais promissoras para criar plataformas multifuncionais “tudo-em-um”, devido à sua capacidade inerente para atuarem na imagiologia biológica, que pode ser combinada com a entrega de medicamentos ou efeitos fototermais/fotodinâmicos. Contudo, a aplicação *in vivo* de nanopartículas metálicas é fortemente condicionada pela sua baixa estabilidade coloidal, perfis citotóxicos desfavoráveis e facilidade em estabelecer interações não específicas no corpo humano. Para colmatar estas desvantagens, as nanopartículas baseadas em metais são, usualmente, combinadas com outros materiais: inorgânicos (p.ex. sílica e

hidroxiapatite), lipídicos (p.ex. lipossomas) ou poliméricos (p.ex. Polietilenoglicol, PEG, ácido hialurónico, HA, e quitosano). Particularmente, a conjugação de metais com polímeros pode apresentar vantagens a nível biológico, melhorando a biocompatibilidade, biodegradabilidade, estabilidade coloidal e a especificidade para o tecido tumoral.

Tomando isto em consideração, o plano de trabalhos desenvolvido durante esta dissertação teve como objetivo desenvolver uma nova metodologia de síntese de nanomateriais de ouro-ácido algínico para aplicação na terapia oncológica. O ouro é um dos metais mais explorados para a produção de nanopartículas metálicas devido às suas características ópticas inerentes, como a ressonância plasmónica de superfície localizadas, a eficiência de conversão luz-calor e a fácil funcionalização. O ácido algínico foi selecionado devido à sua biocompatibilidade e hidrofilicidade, bem como a sua carga negativa, que foi explorada para orientar a formação dos nanomateriais de ouro-ácido algínico. Para este fim, foi promovida a redução e nucleação do ouro na presença de ácido algínico e cloreto de cálcio, que formaram uma rede polimérica, com o ouro reduzido disperso dentro da matriz de nanopartículas. Os nanohíbridos de ouro-ácido algínico apresentaram uma morfologia similar a "estrelas", isto é, com projeções na superfície. Para além disso, a redução do ouro *in situ* induziu um aumento na absorção na região do NIR (*i.e.* 750-1000 nm), quando comparado a nanopartículas de ácido algínico, o que suporta a possível aplicação dos nanohíbridos de ouro-ácido algínico em terapias fototérmicas. Adicionalmente, o tamanho dos nanohíbridos de ouro-ácido algínico permaneceu estável durante três semanas em solução, sendo verificada uma variação semanal média de 1,6% e uma variação de 4,7% depois de 21 dias. As medições do potencial zeta revelaram que os nanohíbridos apresentam uma carga de superfície de -25 ± 4,5 mV, estando de acordo com o perfil aniónico do ácido algínico. Relativamente ao potencial fototérmico, os ensaios *in vitro* mostraram que a irradiação dos nanohíbridos de ouro-ácido algínico com um laser de radiação NIR promove um aumento de temperatura de 11,3 ºC. Por outro lado, os ensaios *in vitro* realizados em fibroblastos humanos (FibH) e células do cancro da mama (MCF-7) revelaram que os nanohíbridos de ouro-ácido algínico eram biocompatíveis, mesmo à concentração mais elevada testada (200 μg mL^{-1}), após 72 h de incubação. Adicionalmente, a internalização dos nanomateriais nas células cancerígenas foi comprovada por microscopia de confocal. Por fim, o efeito fototérmico mediado pelos nanohíbridos de ouro-ácido algínico induziu a diminuição da viabilidade celular de células cancerígenas. Os nanohíbridos de ouro-ácido algínico reduziram a viabilidade das células MCF-7 para ≈27%, quando uma

concentração de nanopartículas de 200 μg mL^{-1} foi utilizada e após 3 ciclos de irradiação com um laser NIR (808 nm, 1,7 W cm^{-2} durante 10 min).

Em suma, os resultados obtidos demonstram que a síntese de nanohíbridos de ouro-ácido algínico foi bem sucedida. Adicionalmente, foi demonstrada a estabilidade destes nanomateriais em solução, o seu potencial fototérmico, e a sua possível aplicação na terapia do cancro. No futuro, a funcionalização dos nanomateriais com agentes de direcionamento (por exemplo, anticorpos ou aptâmeros) e o encapsulamento de fármacos serão explorados para aumentar ainda mais a especificidade para cancro por parte dos nanohíbridos de ouro-ácido algínico e, subsequentemente, permitir o desenvolvimento de terapias combinatórias quimiofotérmicas mais eficazes. Além disso, a realização de ensaios *in vivo* permitirá validar o potencial terapêutico dos nanohíbridos de ouro-ácido algínico.

Abstract

Cancer is still a major burden to public health worldwide with millions of new cases being diagnosed every year. Moreover, this disease also presents a high mortality rate, which can be justified by the difficulties in obtaining an early diagnosis, its rapid progression, and the lack of effectiveness of conventional treatments such as surgery, chemotherapy, and radiotherapy. In fact, the surgical procedure may not ensure the complete removal of the tumor cells, whereas both radiotherapy/chemotherapy present low specificity for cancer cells, causing severe side effects. Therefore, it is urgent to develop and implement new therapeutic approaches with greater selectivity and efficacy.

In recent years, developments in the area of nanotechnology contributed for the emerging of novel solutions for improving the performance of electronics, medical diagnostics, and therapeutics. Particularly, for cancer therapy, the nanoparticles can be explored to develop diagnostic, imaging, therapeutic agents, or even allow the combination of all these functions in one multifunctional system. Such potential rendered the development of several different nanoparticles by varying both the raw material (*e.g.*, polymers, ceramics, lipids, and materials) and the nanoparticles' structure. Among them, metal-based nanoparticles are the most promising materials to create all-in-one multifunctional platforms, due to the inherent bioimaging capacity that can be combined with drug delivery or photothermal/photodynamic effects. Nevertheless, these materials often present suboptimal toxicological profiles and colloidal stability as well as off-target interactions in the human body. To address these issues, metal-based nanoparticles have been often combined with other materials such as inorganic (*e.g.*, silica) and/or organic (*e.g.*, polymers, like Polyethylene glycol, PEG). In this field, the metal-polymer conjugation can be highly advantageous biologically, namely by improving biocompatibility, colloidal stability, and tumor specificity.

Taking this into account, the work plan developed during this MSc dissertation aimed at developing a novel synthesis approach to produce gold-alginic acid nanomaterials for application in cancer therapy. Gold is one of the most explored materials for producing metallic nanoparticles due to their promising optical properties (*e.g.* localized surface plasmon resonance), light-to-heat conversion efficiency, and facile surface functionalization. The alginic acid was selected due to its biocompatibility, hydrophilicity, and negative charge that was explored to guide the nanomaterials

formation. For that purpose, the nanomaterials' production was achieved by promoting gold reduction and nucleation in the presence of alginic acid and calcium chloride. The gold-alginic acid nanohybrids exhibited a spike-like shape with the reduced gold dispersed within the nanoparticle matrix. Moreover, the *in situ* gold reduction led to an improved absorption in the NIR (near-infrared) region, when compared to alginic acid nanoparticles, which indicated the gold-alginic acid nanohybrids potential for application in photothermal therapy. Furthermore, the colloidal stability assays demonstrated that the gold-alginic acid nanohybrids remained stable for 3 weeks, being detected a 4.7% size variation after 21 days. Otherwise, *in vitro* assays performed in human fibroblasts (FibH) and breast cancer cells (MCF-7) revealed that the gold-alginic acid nanohybrids were biocompatible even at the highest tested concentration of 200 μg mL^{-1}, at 72 h of incubation. Additionally, fluorescent-based experiments showed that the nanoparticles can be efficiently internalized by cancer cells. Finally, the irradiation with a near-infrared laser (3 cycles, 808 nm, 1.7 W cm^{-2} for 10 min) resulted in the reduction of the MCF-7 cells' viability to ≈27%, when a gold-alginic acid nanohybrids concentration of 200 μg mL^{-1} was used.

In summary, the obtained results demonstrate the successful synthesis of gold-alginic acid nanohybrids. Moreover, the nanomaterials' colloidal stability, photothermal potential, and possible application in cancer therapy were demonstrated. In the near future, the nanomaterials' functionalization with targeting moieties (*e.g.*, antibodies or aptamers) and the drug loading will be explored to further increase the cancer specificity of the gold-alginic acid nanohybrids and allow the development of more effective chemo-photothermal combinatorial therapies. Furthermore, *in vivo* assays will also be performed to validate the therapeutic potential of gold-alginic acid nanohybrids.

Keywords

Cancer, Nanomaterials, Gold nanoparticles, Alginic acid, Photothermal therapy

List of Publications

Article published in international peer-reviewed journals:

Figueiredo, A.Q.; Rodrigues, C.F.; Fernandes, N.; de Melo-Diogo, D.; Correia, I.J.; Moreira, A.F. Metal-Polymer Nanoconjugates Application in Cancer Imaging and Therapy. *Nanomaterials* 2022, *12*, 3166. https://doi.org/10.3390/nano12183166

Index

Figure Index

Table Index

Lista de Abbreviations

ANOVA	Analysis of varience
AO	Acridine orange
Au-Alg-NH	Gold-alginic acid nanohybrids
BSA	Bovine serum albumin
CA	California
CDT	Chemodynamic therapy
CLSM	Confocal laser scanning microscopy
CT	Computed tomography
DA	Dopamine
ddH2O	Double ionized and filtered water
DLS	Dynamic light scattering
DMEM-F12	Dulbecco's modified eagle medium/nutrient mixture F-12
DMEM-HG	Dulbecco’s modified eagle medium-high glucose
DNA	Deoxyribonucleic acid
DOX	Doxorubicin
EDT	Electrodynamic therapy
EGFR	Epidermal growth factor receptor
EMA	European medicines agency
EPR	Enhanced permeability and retention effect
EtOH	Etanol
FA	Folic acid
FDA	Food and drug administration
FibH	Normal human dermal fibroblast
FITC	Fluorescein 5-isothiocyanate
FL	Fluorescence imaging
GO	Graphene oxide
GSH	Glutathione
GT	Gene therapy
HA	Hyaluronic acid
HSP	Heat-shock protein
ISO	Internation organization for standardization
K-	Negative control
K+	Positive control
KNIR	Non-irradiated control cells

KRB	Krebs ringer buffer
Lf	Lactoferrin
MCF-7	Michigan cancer foundation-7 breast cancer cell line
MDR	Multidrug resistance
MR	Magnetic ressonance
MRI	Magnetic ressonance imaging
MTD	Magnetothermodynamic therapy
MTT	Magnetothermal therapy
N.A.	Not applicable
N.D.	Non disclosed
NCT	National clinical trial
NIPAM	N-isopropylacrylamide
NIR	Near-infrared
NIRFI	Near-infrared fluorescence imaging
NMR	Nuclear magnetic resonance
Olb	Olaparib
p(NIPAM-co-AM)	N-isopropylacrylamide and acrylamide co-polymer
PA	Photoacoustic imaging
PANI	Polyaniline
PBS	Phosphate buffered saline
PDA	Polydopamine
PDT	Photodynamic yherapy
PEG	Poly(ethylene glycol)
PEI	Polyethylenimine
PFA	Paraformaldehyde
PI	Photothermal imaging
PLGA	Poly lactic-co-glycolic acid
PNIPAM	Poly(n-isopropylacrylamide)
POX	Poly(oxazolines)
PTT	Photothermal Therapy
PTX	Paclitaxel
RES	Reticuloendothelial system
RMF	Rotating magnetic field therapy
RNO	p-nitrosodimethylaniline
ROS	Reactive oxygen species
RT	Radiotherapy
S.d.	Standard deviation

SDT	Sonodynamic therapy
SE	Standard Error
TEM	Transmission electron microscopy
TGA	Thermogravimetric analysis
TME	Tumor microenvironment
TPGS	D-alpha-tocopheryl polyethylene glycol 1000 succinate
UV-vis	Ultraviolet-visible
WGA-Alexa Fluor 594®	Wheat germ agglutinin conjugate Alexa 594®
ZnO	Zinc oxide

Chapter 1

Introduction

This chapter is based on the publication entitled: "*Metal-Polymer nanoconjugates application in cancer imaging and therapy*" (2022). Nanomaterials. 12: 3166

1. Introduction

1.1. Cancer development, hallmarks, and conventional cancer therapies

1.1.1. Cancer epidemiology

Cancer is a major healthcare problem worldwide, causing millions of deaths every year [1]. Only in 2020, 19.3 million new cases were diagnosed, and were registered ≈10 million cancer-associated deaths. Moreover, it is estimated that 1 in 5 men or women will develop cancer during their lifetime, and 1 in 8 men and 1 in 11 women will die from cancer every year. The latest projections for 2040 indicate a 47% increase in the global cancer burden, with an expected total of 28.4 million new cases of cancer [2]. In 2020, female breast cancer (2.3 million new cases - 11.7%) surpassed, for the first time, lung cancer (11.4%) as the most diagnosed cancer, followed by colorectal (10%), and prostate cancer (7.3%). However, lung cancer remained the leading cause of cancer-related death (≈1.8 million deaths (18%)), followed by colorectal (9.4%), liver (8.3%), stomach (7.7%), and female breast cancer (6.9%) [2]. In Portugal, accordingly, to a *Direção Geral de Saúde* report from 2017, there has been a 3% increase in cancer incidence per year. This document also predicts that in 2035, cancer incidence and mortality will reach ≈60 thousand and ≈30 thousand cases, respectively [3].

These alarming predictions for cancer incidence and mortality are closely related with the risks factors, such as the increase in the average age of the global population, the exposure to environmental agents (*e.g.*, radiation and pollution), lifestyle (*e.g.*, alcohol consumption, smoking, diet, physical inactivity), as well as the genetical predisposition [4-8]. Furthermore, some infectious agents, like the Hepatitis B virus, Hepatitis C virus, Epstein-Barr virus, Human Papillomavirus, and Human Immunodeficiency virus are known for their oncogenic properties that increase the risk of developing cancer [7, 9].

1.1.2. Cancer development and major hallmarks

Cancer is defined as a complex family of diseases that share different key characteristics in response to genetic and epigenetic alterations, that can ultimately lead to the malignant transformation of normal cells and promote the invasion of the surrounding tissues or other systemic organs [10-12]. Initially, cancer was described as a mass of cells that present an uncontrolled and continuous proliferation, with the ability to invade other tissues of the body [13]. However, cancer is a much more complex and heterogenous tissue, composed of cancer, immune, and stromal cells, and non-cellular elements (extracellular matrix and signalling molecules) that establish dynamic

interactions, constituting the so-called tumor microenvironment (TME) [1, 14]. These cross-talk interactions of TME elements favour the acquisition and maintenance of certain key characteristics ("hallmarks of cancer") by cancer cells, which are essential for cancer development, progression, and metastasis [11].

In 2000, Hanahan and Weinberg described 6 key alterations in cancer cells, *i.e.*, the ability to: 1) evade apoptosis; 2) self-sufficiency in growth signals; 3) insensitivity to anti-growth signals; 4) limitless replicative potential; 5) tissue invasion and metastasis; 6) sustained angiogenesis [13]. The authors updated this list in a subsequent work, adding two emerging hallmarks, deregulating cellular energetics and avoiding immune destruction, and two tumor-enabling features, tumor-promoting inflammation and genome instability [15]. Earlier this year, four more key features were identified (Figure 1), the unlocking of phenotypic plasticity and the formation of senescent cells (emerging hallmarks) and the polymorphic microbiomes and non-mutational epigenetic reprogramming (tumor-enabling characteristics) [11]. These distinctive and complementary hallmarks provide the foundation for a better understanding of cancer biology and the factors that drive tumor growth and metastatic dissemination.

1.1.3. Conventional therapies

The current standard cancer therapy is the combination of surgery with cycles of chemotherapy or radiotherapy [16]. Nevertheless, the therapeutic approach is highly dependent on the tumor's type and stage [17]. Moreover, conventional therapeutics have several disadvantages that limit their effectiveness [18]. The surgical procedure is an invasive and complicated procedure that does not ensure the complete removal of the cancer cells and can lead to damage in surrounding tissues and post-operative complications [19]. In radiotherapy, often occurs the interaction of the highly ionizing radiation with healthy cells inducing severe side effects [19, 20]. Similarly, the lack of tumor specificity by the cytotoxic drugs used in chemotherapy also provokes unwanted non-specific toxic effects [19, 21]. Moreover, cancer cells are also known to develop multidrug resistance (MDR) mechanisms that will decrease chemotherapy efficacy [22]. The most common MDR mechanisms are: 1) Genetic factors (mutations, amplifications, and epigenetic changes); 2) Increased production of growth factors; 3) Expression of cell-protecting genes involved in the xenobiotic metabolism; 4) Enhanced capacity of DNA reparation; 5) Overexpression of drug efflux transporters [23]. Therefore, considering the shortcomings and reduced efficacy of conventional therapies, there is an urgent demand to develop novel and more effective cancer therapies.

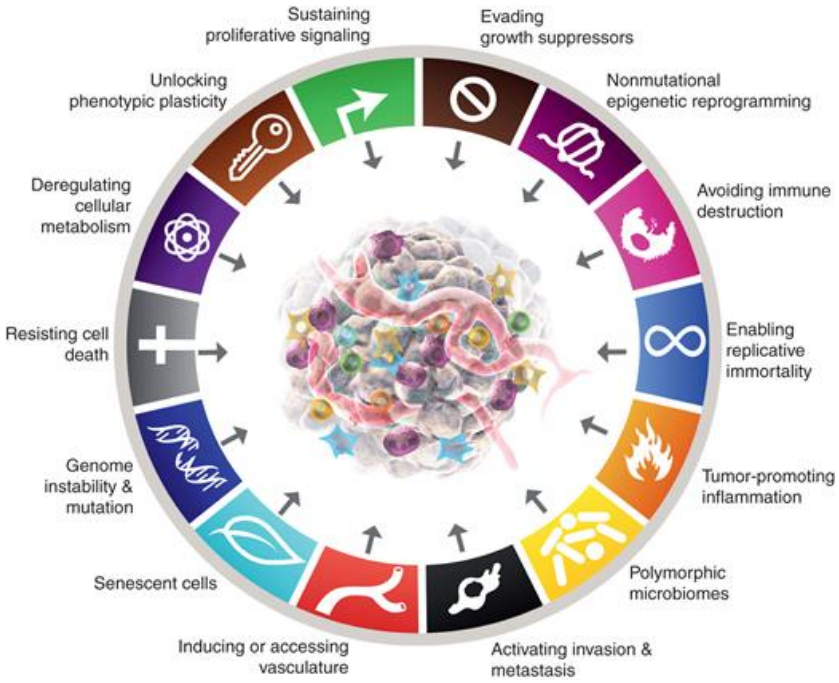

Figure 1 - Hallmarks of Cancer (Adapted from [11]).

1.2. Nanotechnology in cancer therapy

The manipulation of matter at the nanoscale led to the development of various nanomaterials, based on polymers, lipids, ceramics, or metals, that exhibit exciting properties for improving the performance of electronics, medical diagnostics, and therapeutics [24, 25]. Particularly, the application of nanoparticles for cancer therapy led to the development of new alternatives from therapeutics (*i.e.*, drug delivery, photothermal and photodynamic effects) to diagnostic and imaging, leveraging the innate ability of these materials to accumulate in the tumor tissue [26-28]. In fact, this capacity to passively accumulate in the tumor via the enhanced permeability and retention (EPR) effect arises from the nanoparticles' small size [29]. The EPR phenomenon is explained by the rapid and uncontrolled growth of tumors, which leads to the formation of irregular and leaky vasculature (fenestrae with sizes between 200 and 2000 nm) [28, 30]. Therefore, the nanoparticles' size is crucial for their biological performance. Moreover, considering the most common administration route is the intravenous injection, the nanoparticles must also be engineered considering the different barriers in the human body [28]. Nanoparticles with sizes below to 5 nm are rapidly cleared by the kidneys, whereas sizes inferior to 50 nm have higher interaction with hepatocytes, and sizes above 200 nm are easily recognized by the reticuloendothelial system (RES) and entrapped in the spleen [30, 31]. Therefore, sizes between 100 and 200 nm are often referred as optimal for benefiting from the EPR effect and circulate in the human body [32].

Furthermore, other nanoparticles' physicochemical properties (*e.g.*, charge, shape, surface composition) also influence how the nanoparticle behaves *in vivo*. The nanoparticles' surface charge can affect the efficiency and therapeutic outcome by influencing how the nanoparticle interacts with the cells [33]. The particles with a more pronounced surface charge (*i.e.*, values inferior to -10 mV or superior to +10 mV) tend to interact more with RES and proteins (*e.g.* opsonins) during blood circulation [34]. Therefore, a neutral surface charge (*i.e.* surface charge values ± 10 mV) is desirable to increase the blood circulation time and potentiate the nanoparticles' anticancer effect [28, 35].

The nanoparticles' shape (*e.g.*, spheres, cages, rods, stars, sheets) also influences the interaction with the body. Particularly, the shape will determine where the nanoparticles will circulate within the blood vessels. Spherical nanoparticles are found more in the central regions of the blood vessel [28], whereas nanoparticles with an anisotropic shape circulate more in the vessels' periphery [36, 37]. Moreover, some data also indicates that the nanoparticles' shape may also influence cellular uptake and tumor penetration. However, these effects often vary with the nanoparticle's material and the cell type [38, 39].

The nanoparticles' surface chemistry is another important parameter in the nano-bio interactions, namely in the interaction with proteins, such as immunoglobulins, fibrinogens, and opsonins. The protein adsorption at the surface of the nanoparticles is a common phenomenon after intravenous administration, originating the so-called protein corona [40]. This protein corona induces changes in the nanoparticles' size, mediates the aggregation of the nanoparticles, alters the surface charge, and can facilitate clearance by the RES [41, 42]. Therefore, the nanoparticles often are functionalized with different components, such as polymers (*e.g.* Polyethylene glycol, PEG, or Alginate) or biomimetic components (*e.g.* red blood cell membranes) [43, 44], for avoiding protein adsorption and increasing colloidal stability, biocompatibility, biodistribution, and blood circulation time [45-47].

Furthermore, apart from the passive accumulation, the nanoparticles can also be engineered to actively recognize and interact with cancer cells by adding targeting moieties [48]. These targeting agents (*e.g.* antibodies, antibody fragments, peptides) can explore antigen-antibody, host-guest, and ligand-receptor interactions to recognize markers that are uniquely or overexpressed in cancer cells [49-51].

1.3. Metal-polymer nanoconjugates in cancer therapy and imaging

The application of metallic-based nanomaterials (*e.g.*, gold, iron, silver, and copper) has been capturing more attention in recent years due to their characteristic physical (*e.g.*, magnetic behavior, plasmonic resonance, and imaging capacity) and chemical (*e.g.*, radical oxygen species (ROS) generation, and catalytic activity enhancement) properties, which renders them as platforms suitable for creating multifunctional cancer therapeutics [25, 52-55]. Moreover, there are several methodologies described for the synthesis of metallic nanoparticles such as physical or chemical vapor deposition, sol-gel methods, chemical reduction, hydrothermal methods, solvothermal method, laser ablation, and green synthesis processes, allowing the selection of the process most compatible with the available laboratory/industrial conditions and desired physicochemical properties [56-59]. Additionally, metallic nanomaterials surface functionalization, a strategy often used to refine the therapeutics pharmacokinetics, can be performed by well-known and defined methodologies [60]. Thus, the metallic nanomaterials' theranostic potential provides an all-within-one solution for cancer diagnosis, therapy, and real-time monitoring, which ultimately can improve the therapeutic outcome of anticancer therapy [61, 62]. This is the rationale behind various metallic-based nanomaterials under clinical trials, such as Aurolase®, Nanotherm®, and Magnablate®.

Nevertheless, despite the wide number of publications showing the appealing features of metallic-based nanomaterials, their translation into the clinic is still very limited [63]. Such is widely associated with some toxicological issues, lack of colloidal stability, and the establishment of off-target interactions [64]. Additionally, when subjected to high-energy radiations, the metallic nanoparticles often undergo reshaping processes or are even degraded leading to the loss of their therapeutic potential [65]. Therefore, the researchers have been exploring the combination of metallic nanoparticles with other materials inorganic (*e.g.*, silica) and/or organic (*e.g.*, polymers). Particularly, the combination of the metallic nanoparticles' physicochemical properties with the superior biological performance of synthetic or natural polymers arises as a valuable and straightforward approach to develop more effective anti-cancer therapeutics [62, 66]. In the following sections, the application of metallic-polymer nanoconjugates/nanohybrids as a multifunctional all-in-one solution for cancer therapy will be summarized. Initially, the physicochemical properties rendering the metallic nanomaterials' potential to act as

imaging and/or therapeutic agents will be described. Then, an overview of the main advantages of metal-polymer conjugation as well as the most common structural arrangements will be provided. Moreover, the application of metallic-polymer nanoconjugates/nanohybrids made of gold, iron, copper, and others in cancer therapy will be discussed, providing also an outlook of the current solution in clinical trials.

1.3.1 Metallic nanoparticles applications and therapies

Nanosized metals present optical and electrical properties that differentiate them from other nanomaterials and have been supporting their application in biomedicine, such as the development of biosensors (*e.g.*, diagnosis of viruses using colloidal gold nanoparticles), bioimaging agents (*e.g.*, iron oxide-based contrast agents), catalysts, mechanical reinforcement, and drug delivery system or other therapeutics. Moreover, these unique set of characteristics can be explored to create more effective antitumoral nanomedicines. The high density and X-ray attenuation capacity of metallic nanoparticles renders to them the intrinsic capacity to be applied as contrast agents for bioimaging applications [67]. Up to now, several studies available in the literature have already shown that metallic nanoparticles provide a higher contrast enhancement in X-ray computed tomography (CT) imaging than the iodine-based contrast agents conventionally used in the clinic [68-72]. On the other hand, nanosized metals, such as gold, silver, and copper, show a pronounced plasmonic resonance phenomenon, *i.e.*, the collective oscillation of the conduction band electrons in metal-based nanomaterials in response to the incident photons [73]. This interaction can lead to light absorption or scattering and is dependent on the size, morphology, distance, and dielectric constant of the metallic nanoparticles and surrounding medium [74-76]. In turn, the excited surface electrons can decay to the ground state via different processes (*e.g.*, electron-to-photon, electron-to-electron, and electron-to-phonon energy conversion), being the two most common events the release of the absorbed energy in the form of light or heat [77]. The former is often explored to enhance the quantum efficiency and photostability of fluorophores, allowing the detection of lower quantities of biomarkers used in biosensing or bioimaging [78]. The latter is the funding stone for the application of metallic nanoparticles in cancer hyperthermia/photothermal therapy [79]. However, it is essential to tailor the nanomaterials to interact specifically with near-infrared (NIR) radiation, a region of the spectra where the major biological components (*e.g.*, collagen, hemoglobin, and water) have the lowest or insignificant absorption [80]. Such will reduce the off-target interactions and guarantee a site-specific activation of the metallic nanomaterials. Then, the heat generated by the light-nanoparticles interaction can mediate the destruction of the cancer cells [81, 82]. The elevation of the tumor

temperature to values superior to 45 °C provokes irreversible damage to cancer cells (*e.g.*, DNA degradation, cell membrane disruption, protein denaturation) leading to cell death (*i.e.*, tumor ablation). Otherwise, if mild temperature increases are achieved (*i.e.*, between 40 and 45 °C), the cell damages are less pronounced and often reversed by the cell repair mechanisms [28, 83, 84]. Nevertheless, this creates a time window where the cancer cells are more sensitive to the action of other therapeutic modalities, such as chemotherapy [85]. Furthermore, metallic nanomaterials, such as those composed of iron, nickel, and cobalt, can also present magnetic properties allowing also their application as contrast agents (magnetic resonance imaging (MRI)) and in tumor magnetic hyperthermia [86]. This capacity to be magnetically manipulated by external magnetic fields is also explored to guide these metallic nanomaterials in the human body and promote a tumor-specific accumulation [87, 88]. At the tumor site, the utilization of alternating magnetic fields will promote the nanoparticles' vibration and consequently a localized temperature increase will be obtained [89].

Metallic nanomaterials have also shown the capacity to mediate the formation of ROS [64]. This oxidative stress can influence several cellular processes/structures, *e.g.*, intracellular calcium concentrations, activate transcription factors, induce DNA damage, and lipid peroxidation (cell membrane disruption), and increased amounts of ROS are highly cytotoxic [64]. The mechanism of ROS generation by metallic nanomaterials is influenced by their physicochemical properties (*e.g.*, size, chemical structure, surface area, and charge) [90]. Generally, metallic nanomaterials act as the reactant or catalyst for the reduction of molecular oxygen to water, which yields the production of ROS, such as superoxide radicals and hydroxyl radicals [91]. The ROS generation of metallic nanomaterials can be further boosted by light absorption [92]. During this process, the electrons transit to higher energy bands facilitating the reaction with water or molecular oxygen and consequently the ROS generation, a process denominated by photodynamic effect [93, 94].

Despite the imaging and therapeutic potential of metallic nanoparticles, the *in vivo* application and translation to the clinic are severely hindered by their low colloidal stability, high reactivity, the formation of the protein corona, and high cytotoxicity [95-97]. Therefore, to overcome these limitations researchers have been combining the superior physicochemical features of metallic nanoparticles with the increased biological properties (*e.g.*, biocompatibility, enhanced blood circulation time, targeting capacity) of synthetic and natural polymers, often referred to as metal-polymer nanocomplexes or nanohybrids.

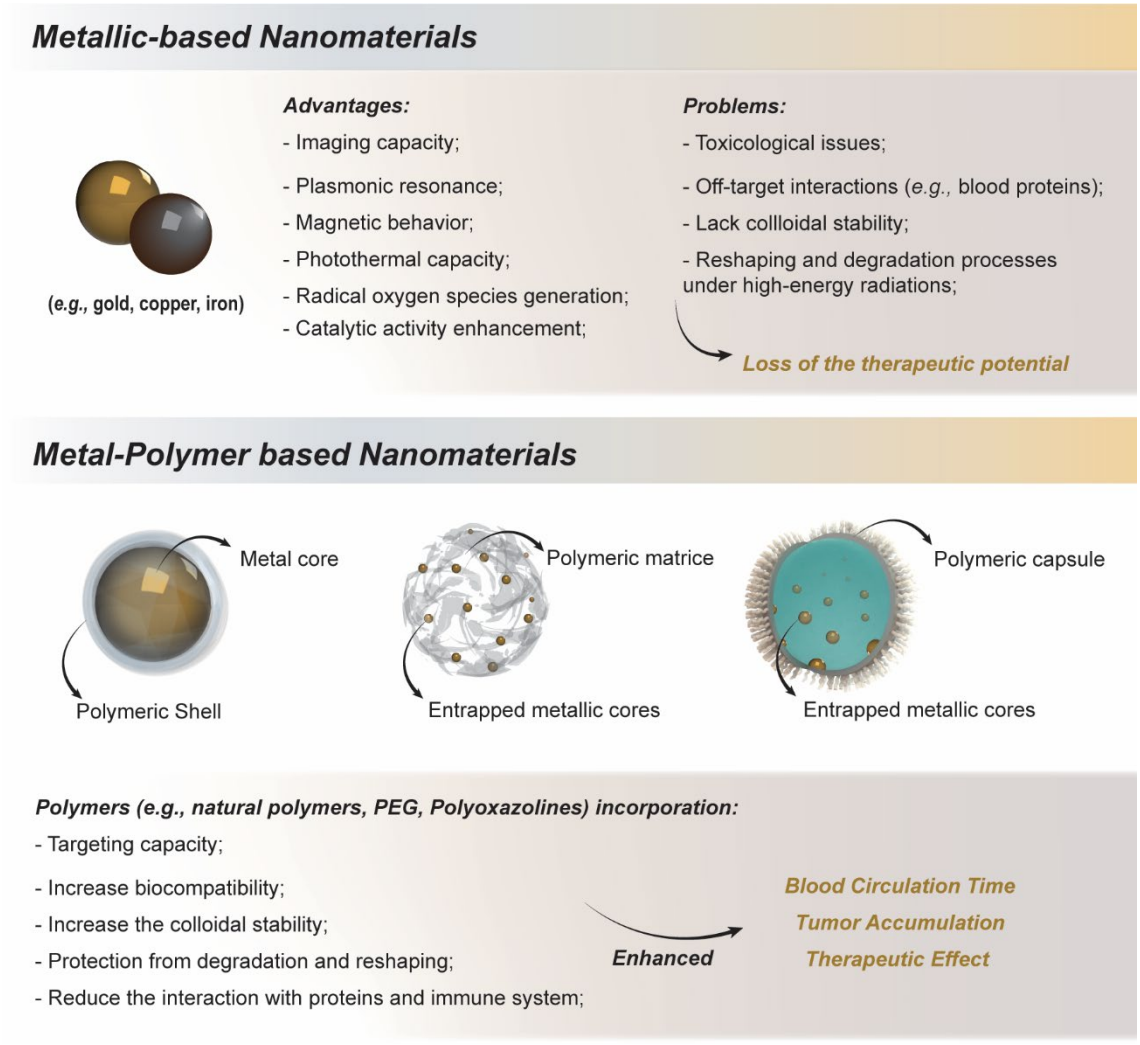

Figure 2 - Overview of the properties of metallic nanoparticles, advantages of the polymers' inclusion, and representation of the most common structural organizations of the metal-polymer nanohybrids/complexes.

1.3.2. Metal-polymer based nanomaterials

The metal-polymer nanocomplexes or nanohybrids are a class of nanomaterials that aim to address the biological bottlenecks of the metallic nanoparticles' administration in humans. For that purpose, several strategies have been explored to create these new nanomaterials (Figure 2), namely, the i) surface coating of metallic cores (*e.g.*, physical linkage and layer-by-layer), ii) entrapment of metallic cores within polymeric matrices (*e.g.*, nanoparticle *in situ* growth or post-synthesis entrapment), and iii) the utilization of polymeric capsules [98-100]. One of the main rationales behind the introduction of polymers is to increase the colloidal stability of metallic nanoparticles and avoid protein adsorption during the nanoparticles' circulation in the blood [101, 102].

Highly hydrophilic polymers are often associated with improvements in the nanoparticles' blood circulation time, namely by minimizing the nanoparticle-protein interaction, avoiding nanoparticles' aggregation as well as the size and charge changes, and reducing the recognition by the immune cells [103, 104]. For this purpose, polymers such as poly(ethylene glycol) (PEG), poly(oxazolines) (POX), and poly(zwitterion)s have been excelling in enhancing the nanoparticles' blood circulation [105]. The PEG and POX anti-fouling properties, which are attributed to two main events i) the steric repulsion and ii) the water barrier, difficult the nanoparticles-proteins interaction avoiding the formation of a protein corona that negatively impacts the nanomaterials' biological performance [106, 107]. In turn, the zwitterionic polymers present overall electrostatic neutrality and high chain hydration that confer to them a stealthing capacity [108, 109]. The higher blood circulation times associated with the utilization of these polymers will increase the nanomaterials' probability to accumulate and interact with the tumor cells, which can be essential for achieving superior antitumoral effects [110]. On the other hand, the natural and synthetic polymers can also imprint a stimuli-responsive (*e.g.*, pH, temperature, and enzymatic) behavior on the metallic-based nanomaterials, which can be particularly advantageous for controlling drug delivery [79, 111-114]. In this regard, the heat generated by the nanomaterials (*e.g.*, PTT and magnetic hyperthermia) can be also explored to induce phase changes in the polymers (*e.g.*, Poly(N-isopropylacrylamide) (PNIPAM)) or increase their solubility, which will trigger the drug release [114, 115]. Additionally, at the tumor site, the metal-polymer nanocomplexes/nanohybrids will also have an impact on the physiological conditions that can be explored to trigger the drug release, such as an acidic pH, overexpression of certain enzymes (*e.g.*, matrix metalloproteinases), and an increased RedOx environment [111, 113, 116]. Apart from the passive accumulation of the nanomaterials at the tumor site, usually dependent on the EPR effect, the polymers or other targeting moieties can confer a specific recognition of molecules overexpressed in the tumor tissue [28, 117]. This higher specificity towards cancer cells will favor the nanomaterials accumulation in these areas as well as the nanomaterials-cancer cell interaction [118]. Therefore, the metal-polymer nanocomplexes or nanohybrids show the potential to create novel and more effective anticancer therapeutics. In the following section, the application of metallic-polymer nanoconjugates/nanohybrids made of gold, iron, copper, and others in cancer therapy will be overviewed, showing the therapeutic modalities that each metal nanoparticle allows to explore.

1.3.2.1 Gold-polymer conjugates

Gold nanoparticles are one of the most explored metallic nanomaterials for biomedical applications, from bioimaging to drug delivery [119-121]. The applicability of gold nanomaterials in bioimaging is demonstrated in different works in the literature, principally as a contrast agent for CT imaging [122]. For example, Xi and co-workers observed that, when an X-ray beam of 100 KeV is used, gold nanoparticles present an absorption coefficient 2-times superior to that obtained with iodine (a conventional contrast agent used in the clinic) [123]. In turn, the pronounced surface plasmon resonance of gold nanoparticles has been supporting the development of novel photothermal therapies for cancer therapy (Table 1). This phenomenon can be fine-tuned to enhance the gold nanoparticles' absorption in the NIR region (700-1100 nm) by optimizing the nanoparticles' size and/or shape (*e.g.*, spheres, cages, stars, and rods) [83, 124]. *Per se*, the gold nanospheres application in cancer photothermal therapy (PTT) is limited since its absorption peak is in the 500 to 550 nm region [125]. However, the organization of gold nanospheres in nanoclusters or shells renders a shift in the absorption spectra to the NIR region [25, 28]. This change in the gold nanoparticles' optical properties is attributed to the coupling of the plasmon resonance of adjacent gold nanospheres [126]. Therefore, the fine-tuning of the gold nanoclusters or shells' absorption spectra can be achieved by optimizing the nanospheres' size and interparticle distance [25]. In turn, the surface plasmon resonance in non-spherical gold nanoparticles varies with the nanoparticle surface [127, 128]. For example, the two different surfaces in gold nanorods, longitudinal and transversal surfaces, originate two absorption bands. The transversal surface leads to an absorption band in the 500-550 nm region of the spectra, whereas the longitudinal surface originates an absorption peak that can be fine-tuned from the visible to the NIR region of the spectra [129, 130]. This peak generated by the longitudinal surface resonance is determined by the aspect ratio of gold nanorods (*i.e.*, quotient between length and width) [131]. Otherwise, the surface plasmon resonance of gold nanostars is defined by the particle's core size, the number of tips, as well as the tips' length and width [25]. Therefore, the gold nanoparticles' plasticity and fine-tunning ability to present a high absorption efficiency in the NIR region of the spectra propelled their application in the cancer PTT.

Nevertheless, despite the theragnostic potential of gold nanoparticles, their direct application in the human body is hindered by their high affinity to establish interactions with thiol groups, which favors the interaction with different biomolecules and lead to the nanoparticles' aggregation [126]. Moreover, the gold nanoparticles can also be degraded when exposed to high-energy radiations, such as those used in CT imaging and

PTT, causing the loss of their bioactivity [132]. Furthermore, several reports in the literature also describe that gold nanoparticles are strongly accumulated in the kidneys, causing nephrotoxicity, and may also trigger the lysis of red blood cells [124]. To address these issues, researchers have been exploring the development of gold-polymer nanocomplexes or nanohybrids to increase colloidal stability, biocompatibility, and even tumor specificity.

Peng and colleagues demonstrated the applicability of gold-based nanomaterials in bioimaging by following the biodistribution and tumor accumulation of PEGylated dendrimer-entrapped gold nanospheres [133]. In fact, the authors reported that these nanomaterials have an attenuation intensity higher than Omnipaque (an iodine-based contrast agent), which allowed them to follow the PEGylated dendrimer-entrapped gold nanoparticles in the blood circulation, after intravenous injection, as well as to perform the CT imaging of SPC-A1 xenograft tumors. Moreover, the authors reported that the PEGylated dendrimer-entrapped gold nanoparticles had a half-decay time in the blood circulation of 31.76 h, which was to 2.5-times higher than that of bare gold nanorods previously reported. Furthermore, Gu *et al.* produced RGD-modified mPEG-PLGA nanocapsules containing gold nanoclusters and indocyanine green for the imaging and PTT of breast cancer [134]. The loaded mPEG-PLGA nanocapsules were formed via a water-in-oil-in-water emulsion using sonication, i) the first emulsion consisted of the water phase with gold nanoclusters and the oil phase with indocyanine green and the mPEG-PLGA. In the second emulsion, the mPEG-PLGA nanocapsules were further modified with poly(vinyl alcohol) and poly(acrylic acid), allowing the subsequent functionalization with RGD peptide via carbodiimide chemistry. The authors demonstrated that both one-photon and two-photon imaging techniques could be used to follow the nanocapsules in 4T1 tumor-bearing BALB/c mice. Moreover, the RGD-modified nanocapsules showed a preferential accumulation in U87-MG cancer cells (overexpressing $\alpha v\beta_3$ integrins), when compared to MCF-7 cancer cells (low expression of $\alpha v\beta_3$ integrins), leading to the almost complete ablation of the cancer cells after irradiation with a NIR laser (808 nm, 2 W cm^{-2}, for 5 min). Feng and co-workers developed two different tumor-targeted gold nanocages for the combinatorial chemo-PTT of breast cancer [114]. For that purpose, pH-responsive gold nanocages were formulated via electrostatic interaction between the poly(acrylic acid) and the surface of the particles, entrapping the gold particles in the polymeric chains (p_AAu nanoparticles) and loaded with Erlotinib (Erl), an epidermal growth factor receptor (EGFR) inhibitor. In turn, temperature-responsive gold nanocages were produced by reacting them with the thiol-terminated N-isopropylacrylamide (NIPAM) and acrylamide (AM) (p(NIPAM-

co-AM) co-polymer (p_NAu nanoparticles) and subsequently loaded with doxorubicin (Dox). The p_AAu nanoparticles showed a pH-triggered Erl release due to the protonation of poly(acrylic acid) in acidic pH (*i.e.*, loosening of the polymeric barrier), 4.5, 24.8, 44.1, or 66.3% Erl released after 6 h at pH 7.4, 6.5, 6, or 5. Otherwise, the Dox-loaded p_NAu nanoparticles were responsive to the irradiation with a NIR laser (808 nm, 0.5 W cm^{-2}, for 10 min) and consequent increase in temperature (*i.e.*, superior to 45 ºC, a value higher than the lower critical solution temperature). The authors reported a 46.2% of Dox released in 10 h, after a 10 min NIR laser irradiation, contrasting with the 5% detected in the absence of NIR irradiation. The *in vivo* studies performed in MCF-7 and A431 tumor-bearing mice demonstrated a passive and preferential accumulation in the tumor tissue (Figure 3). Moreover, the combinatorial therapy led to the reduction of A431 tumors' size by 98%, after 14 days, whereas in MCF-7 tumors (low expression of EGFR), these nanomaterials only slowed the tumor growth.

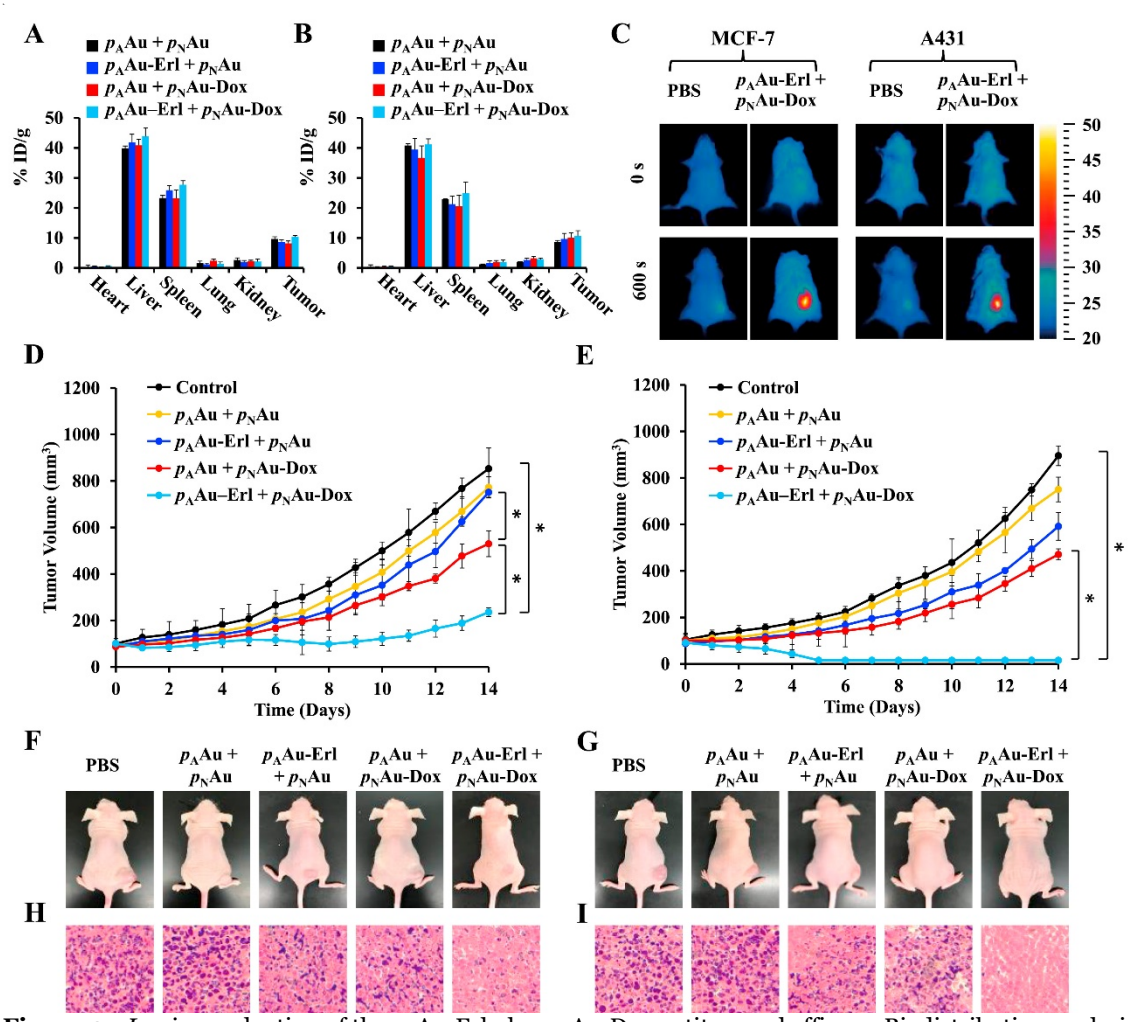

Figure 3 - *In vivo* evaluation of the p_AAu-Erl plus p_NAu-Dox antitumoral efficacy. Biodistribution analysis of p_AAu + p_NAu, p_AAu-Erl + p_NAu, p_AAu + p_NAu-Dox, and p_AAu–Erl + p_NAu-Dox (12.4 Au mg.kg^{-1} of mouse, Erl:Dox = 1:1) in MCF-7 (A) and A431 (B) tumor-bearing mice. Infrared thermal images of MCF-7 and A431 tumor-bearing mice before and after NIR laser irradiation (808 nm, 0.5 W cm^{-2}, for 10 min) (C). Analysis of the tumor growth curve in MCF-7 (D) and A431 (E) tumor-bearing mice. Photos and histological analysis of

MCF-7 (F and H) and A431 (G and I) tumor-bearing mice. Reprinted with permission from [114]. Copyright (2019) Elsevier.

1.3.2.2. Iron-polymer conjugates

The utilization of iron oxide nanoparticles can be explored in different biomedical applications, such as drug delivery, hyperthermia, and magnetic resonance imaging. Similar to gold nanoparticles, iron oxide can be produced in different shapes, such as spherical, rod-like, and cubical [135, 136]. These nanoparticles (Fe_2O_3 and Fe_3O_4), when their size is inferior to 20 nm, present a superparamagnetic behavior at room temperature, *i.e.*, the magnetization of the nanoparticles is close to 0 in the absence of an external magnetic field [137, 138]. The iron oxide nanoparticles magnetism has rendered to these nanomaterials a widespread application in cancer therapy (Table 2), namely as contrast agents for magnetic resonance imaging: Feridex®, Resovist®, and Endorem®. The data available in the literature indicates that iron oxide nanoparticles are less toxic than the conventionally used gadolinium-based contrast agents, without presenting significant losses in the imaging capacity [137]. Moreover, the magnetic properties of iron oxide nanoparticles have also been explored to direct the accumulation of the nanoparticles, specifically towards the tumor tissue, and in certain cases mediate a hyperthermic effect [139, 140]. The former explores the application of an external magnetic field to guide the nanoparticles and promote their accumulation in the target tissue [141]. The latter employs an alternating magnetic field to induce the oscillation of iron oxide nanoparticles, which in turn generate heat [139]. This hyperthermic effect is dependent on the magnetic properties of the nanoparticles as well as on the frequency and intensity of the alternating magnetic field [142, 143]. However, the biological application of iron oxide nanoparticles is hindered by their limited colloidal stability, tending to agglomerate when in contact with biological fluids [144]. With this in mind, Xu *et al.* prepared GSH-responsive Hyaluronic acid-coated small iron oxide nanoparticles (HIONPs) for the diagnosis of liver metastases [145]. The nanoparticles were formed via a one-pot method promoting the oxidation of ferrous ions to create iron oxide nanoparticles that were coated with hyaluronic acid modified with dopamine through the establishment of phenol–metal coordination interactions. The *in vitro* measurements in a 0.52 T NMR instrument showed that the HIONPs have a longitudinal proton relaxivity (r_1) of 41.3 Fe mM^{-1} s^{-1}, indicating the applicability of HIONPs as T_1 MRI contrast agents. Such was confirmed using a 3 T MR scanner where the HIONPs led to higher T_1-weighted magnetic resonance signals and lower T_2-weighted magnetic resonance signals when the Fe concentration increased from 0 to 0.2 mM. Moreover, the application of HIONPs (Fe - 0.03 mmol kg^{-1}) in mice with B16F10, 4T1, and CT26 liver metastases allowed the metastases detection via MRI, showing the highest contrast-to-

noise ratio 1 h after injection. This capacity is attributed to the higher GSH concentration in the mice liver tissue (*i.e.*, 11 to 76-times higher) when compared to the tumor/metastases. The higher GSH concentration promotes the removal of the hyaluronic acid coating and consequent nanoparticle aggregation, which led to a significant decrease in the r_1 value. In this way, the hepatic tissues became dark whereas the tumor/metastases are bright in the MRI. Moreover, the authors also described that the HIONPs presented a higher imaging capacity than Primovist® (Gd-based imaging agent), where the metastases and surrounding liver tissue presented a similar contrast-to-noise ratio. In another work, Xiao and co-workers developed ultrathin vesicles with multimodal imaging capacity for the combinatorial chemo-PTT of cancer [146]. For that purpose, ultrasmall superparamagnetic iron oxide nanoparticles, cisplatin, and liquid perfluorohexane were encapsulated in PLGA nanovesicles, followed by the formation of an ultrathin silica layer to prevent leakage. Then, the surface of the particles was modified with polyaniline (a photothermal agent) and functionalized with R8-RGD. In these nanoparticles, the iron oxide acted as a T_2-weighted magnetic resonance contrast agent, with a transverse relaxivity (r_2) value of 258.5 Fe mM^{-1} s^{-1}, 3-times superior to the iron oxide nanoparticles alone. Moreover, the *in vivo* studies in A549 tumor-bearing mice showed that the administration of the PLGA vesicles containing the iron oxide nanoparticles allows the monitoring of the changes in the tumor cellularity via MRI. Additionally, the chemo-photothermal combinatorial treatment led to a significant regression, close to 97%, of the tumor volume in 21 days. Chen and colleagues produced a dual-targeted magnetic iron oxide nanoparticle for the imaging and hyperthermia of breast tumors (Figure 4) [147]. The iron oxide nanoparticles were coated with a DSPE-PEG2000 shell and then modified with RGDyK (neovascular endothelium targeting) and D-glucosamine (glucose transporter affinity) via carbodiimide chemistry. The authors observed that the combination of magnetic and active targeting approaches resulted in the best contrast effect on T_2-weighted MRI from 3 to 48 h, showing the tumor region completely dark due to the accumulation of the nanoparticles. The tumor/normal tissue signal ratio at 48 h for active targeting strategies was 0.6 whereas for the magnetic plus active targeting combination this value was inferior to 0.3, showing a higher difference in the signal obtained in the tumor and normal tissues. Moreover, the utilization of alternating current magnetic fields (1.485×10^9 Am^{-1} s^{-1}), focused on the tumor region, induced a temperature increase to 44 °C, which successfully slowed the growth of 4T1 tumors when compared to the control group (*i.e.*, the relative tumor volume of 500 and 200% for control and iron oxide groups, respectively).

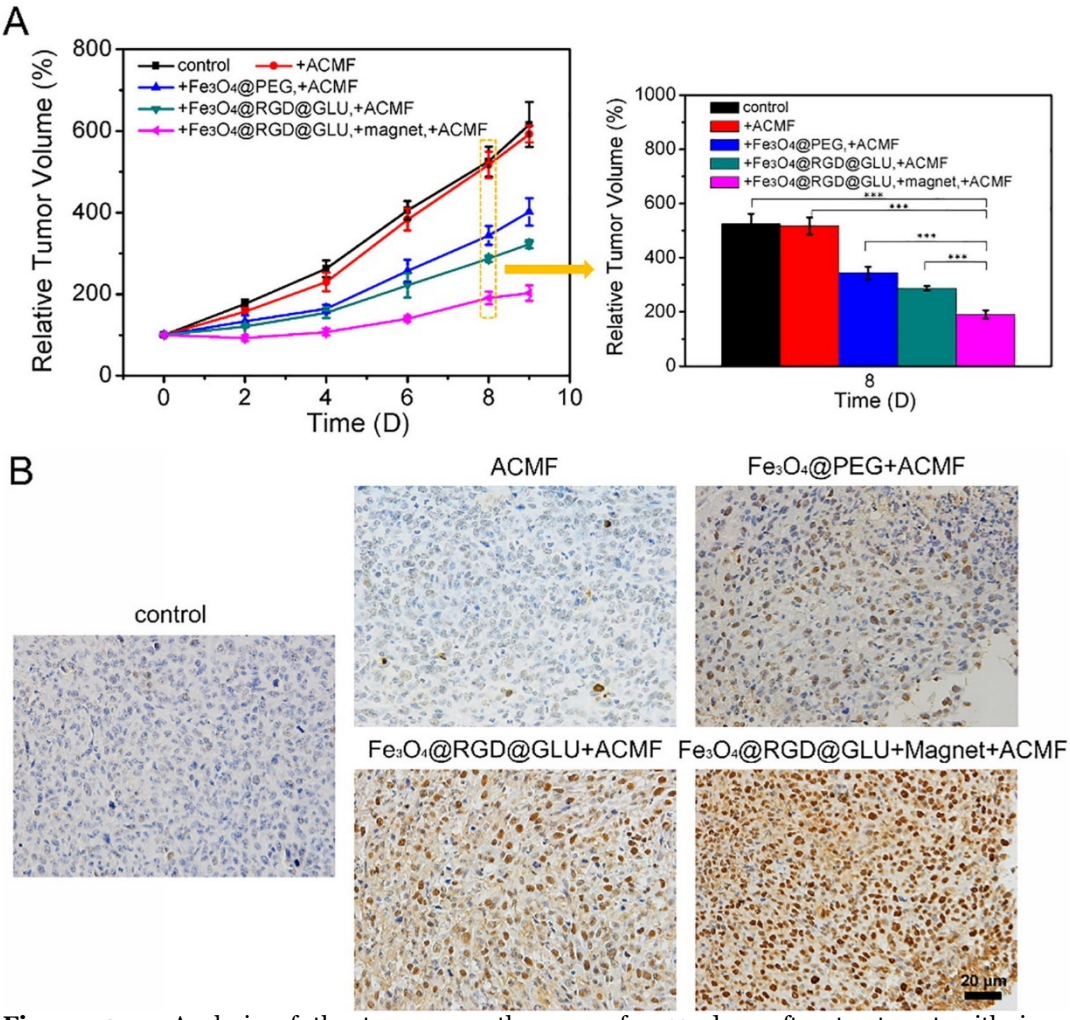

Figure 4 - Analysis of the tumor growth curves for 10 days after treatment with iron oxide Fe_3O_4@RGD@GLU exposed to an alternating current magnetic field and an external permanent magnet, mean ± SE and n=5 (A). TUNEL histological analysis of mice tumors at day 9. Reprinted with permission from [147]. Copyright (2019) Elsevier.

1.3.2.3. Copper-polymer conjugates

Copper nanomaterials emerged in recent years as promising inorganic nanoparticles for biomedical applications (Table 3). Copper is a transition metal and can be engineered to form various nanomaterials, such as copper oxides, copper selenides, and copper sulfides [148-150]. Among them, copper sulfides have been the most explored due to the simple synthesis process and high NIR absorbing capacity allowing their application in cancer PTT [83]. On the other hand, the copper nanomaterials can also be used as Fenton-like reagents mediating the formation of ROS (*i.e.*, chemodynamic therapy) [151]. Moreover, the generation of ROS can also be stimulated under light irradiation (photodynamic therapy (PDT)) [152]. However, copper is often defined as more toxic than iron and gold, which makes undesirable the release of copper ions in the human body [153, 154]. With that in mind, *Li et al.* showed that the surface functionalization with an amphiphilic polymer, poly(isobutylene-alt-maleic anhydride)(PMA), enhances the colloidal stability

of copper telluride nanoparticles without visible agglomeration for periods superior to one month [155]. Furthermore, *in vitro* studies performed in 3T3 fibroblasts showed significant cytotoxicity after irradiation with a NIR laser (830 nm, 0.5 mW cm^{-2}, for 2 s). In another work, Li and colleagues developed a PEGylated copper sulfide nanoparticle for the simultaneous PDT and PTT of lung cancer (Figure 5) [156]. For that purpose, thiolated-PEG was reacted with the copper sulfide nanoparticles rendering the PEGylated nanoparticles. The authors observed that the nanoparticles' irradiation (30 μg mL^{-1}) with a NIR laser (808 nm, 1 W cm^{-2}, for 10 min) reaches temperatures superior to 42 ºC. Moreover, the authors also observed the continuous quenching of the p-nitrosodimethylaniline (RNO) absorption under NIR irradiation, indicating the generation of ROS during this period. Moreover, the *in vivo* studies in SPC-A-1 tumor-bearing mice showed that the combination of PDT and PTT decreases tumor growth, observing a 5% increase in the tumor volume at day 14 after administering PEGylated copper sulfide nanoparticles (30 μg mL^{-1}) plus NIR. Similarly, Shi *et al.* produced a PEGylated copper sulfide nanoparticle modified with RGD to target metastatic gastric cancer [157]. The nanoparticles were formed by the reaction of thiolated-PEG-COOH and copper sulfide, followed by the RGD modification using carbodiimide chemistry. The obtained nanoparticles showed computed-tomography contrast capacity similar to the Iodixanol (a clinically used contrast agent). Furthermore, the irradiation of the nanoparticles (60 μg mL^{-1}) with a NIR laser (808 nm, 1 W cm^{-2}, for 5 min) led to a temperature increase to 60 ºC. In the *in vivo* studies, the authors observed that the RGD-modified PEGylated copper sulfide nanoparticles allowed the identification of MKN45 tumors and metastasis in sentinel lymph nodes through T_2-weighted magnetic resonance images. Moreover, the NIR laser irradiation (808 nm, 1 W cm^{-2}, for 10 min) promoted the increase in tumor/metastases temperature to 57 ºC, leading to the complete ablation of the metastatic MKN45 tumors (sentinel lymph nodes weight similar to the healthy ones, 2.5 mg).

1.3.2.4. Zinc, platinum, and silver-polymer conjugates

Apart from the previously presented gold-, iron-, and copper-based nanomaterials other metals have also been explored to create novel and more effective anticancer therapeutics (Table 4). Zinc-based nanoparticles, particularly zinc oxide (ZnO), are considered relatively biocompatible and generally regarded as safe. These nanoparticles present photoluminescence properties and a band gap that facilitates the interaction with oxygen and hydroxyl ions prompting the generation of superoxide and hydroxyl radicals (Table 4) [158, 159]. Moreover, this ROS generation shows a certain selectivity towards cancer cells, decreasing the potential for inducing side effects [160]. Song and co-workers

functionalized ZnO nanoparticles with polyvinylpyrrolidone for application in the imaging and therapy of colon cancer [161]. These authors reported that the surface functionalization maintained the nanoparticles stable for 14 days, whereas non-coated ZnO nanoparticles aggregated after 3 days, without impacting the ROS generation capacity. Moreover, the authors also observed that the administration of the polyvinylpyrrolidone-coated ZnO nanoparticles, at a concentration of 50 μg mL^{-1}, reduced the viability of SW480 cancer cells to 54% due to ROS generation. In turn, the ROS generation was boosted by the irradiation with UV light, with cell viability of 15% at a concentration of 50 μg mL^{-1} (IC_{50} of 21.688 μg mL^{-1}). This PDT capacity was also observed in the SW480 tumor-bearing mice, where the nanoparticles plus light treatment slowed the tumor growth for 28 days, with a tumor inhibition rate of 61.1%.

Platinum (Pt) is a catalytic noble metal that has been explored in cancer therapy, namely in the form of chemotherapeutic drugs containing platinum atoms such as cisplatin and derivatives [162]. The utilization of platinum nanoparticles is focused on the release of platinum ions that will induce DNA damage and provoke cell death [163]. Additionally, the platinum nanoparticles can also mediate the generation of ROS or act as photothermal agents [164, 165]. Chen and colleagues developed PEGylated porous platinum nanoparticles loaded with Dox for application in breast cancer therapy [166]. In the synthesis process, Pluronic F127 was used as a surfactant for the platinum nanoparticles and then reacted with thiolated-mPEG. This surface modification enhanced the solubility and stability of the platinum nanoparticles. Moreover, the authors also reported that the presence of a 10 mHz square wave AC field (10 mA) further enhanced the ROS generation capacity. In turn, the combination of Dox delivery and ROS generation induced the regression of 4T1 tumors, showing a tumor growth inhibition of 95.5% after 14 days. Zhu and co-workers prepared sodium hyaluronate stabilized platinum nanoparticles (HA/Pt) for mediating a photothermal effect [167]. Apart from the nanoparticle stabilization, the HA functionalization increased the nanoparticles' specificity towards the MDA-MB231 cancer cells (overexpression of CD44), when compared to the uptake by NIH3T3 cells (low expression of CD44). Furthermore, the *in vivo* studies in MDA-MB231 tumor-bearing mice revealed that upon irradiation with a NIR laser (808 nm, 1 W cm^{-1}, for 10 min), the HA/Pt nanoparticles induced an increase in the temperature of the tumor to 44 ºC, which translated to a reduction in the tumor growth for 14 days.

Silver (Ag) is a noble metal with vast applications being widely applied in the biomedical field as an antimicrobial agent [168]. The silver nanoparticles can mediate ROS

formation and consequently induce lipids peroxidation, protein oxidation, and DNA damage [169, 170]. Park and co-workers developed indocyanine green-loaded silver nanoparticles functionalized with PEG and BSA for application in cancer PTT [171]. The BSA was used to stabilize the produced silver nanoparticles, followed by the reaction with NHS-PEG for obtaining the functionalized silver nanoparticles. The authors reported that the PEG-BSA silver nanoparticles were stable in solution for at least 5 days after the synthesis. Moreover, the combination of indocyanine green-silver nanoparticles resulted in a more stable photothermal effect, reaching temperatures of ≈45 ºC even after 3 irradiations with a NIR laser (885 nm, 1.3 W, for 10 min). The *in vivo* studies performed in B16F10 tumor-bearing mice showed a preferential accumulation in the liver, kidney, and tumors and upon irradiation (885 nm, 0.95 W for 20 min), the tumors' temperature reached 49 ºC. This photothermal effect led to the tumors' ablation after 4 days.

1.3.3. Clinical trials

Since the 90s, more than 50 nanomedicines were approved by the Food and Drug Administration (FDA) and are currently on the market [172]. However, in the last decade, only a small number of formulations successfully reached the clinic for cancer treatment, a fact that is in part related to the poor pharmacokinetics of the nanomaterials [173]. The latest data indicates that less than 1% of the administered nanoparticles reach the tumor site [174]. Nevertheless, most of the approved nanomedicines are based on liposomes, protein nanoparticles, nano-emulsions, and metal oxide nanoparticles.

Particularly, iron oxide nanoparticles' clinical utility is demonstrated by the FDA approval for application in cancer diagnosis, hyperthermia, and iron deficiency anemia. Among them, it is worth highlighting the various contrast agents based on iron oxide nanoparticles commercially available for MRI, such as Feridex®, Resovist®, and Endorem®. Moreover, there are more systems under clinical trials such as Magnablate® and Nanotherm® (Table 5). The former is an iron oxide nanoparticle developed for magneto-hyperthermia applications that underwent a Phase 0 clinical trial (ClinicalTrials.gov Identifier: NCT02033447), with 12 participants, for the thermoablation of prostate cancer (no results are yet available) [175]. In turn, Nanotherm® is also based on an aqueous suspension of iron oxide nanoparticles and was already approved by the European Medicines Agency (EMA) for brain tumor treatment [83]. Moreover, recently a new clinical trial (ClinicalTrials.gov Identifier: NCT05010759; still recruiting) was announced to study the application of Nanotherm® in the ablation of prostate carcinoma.

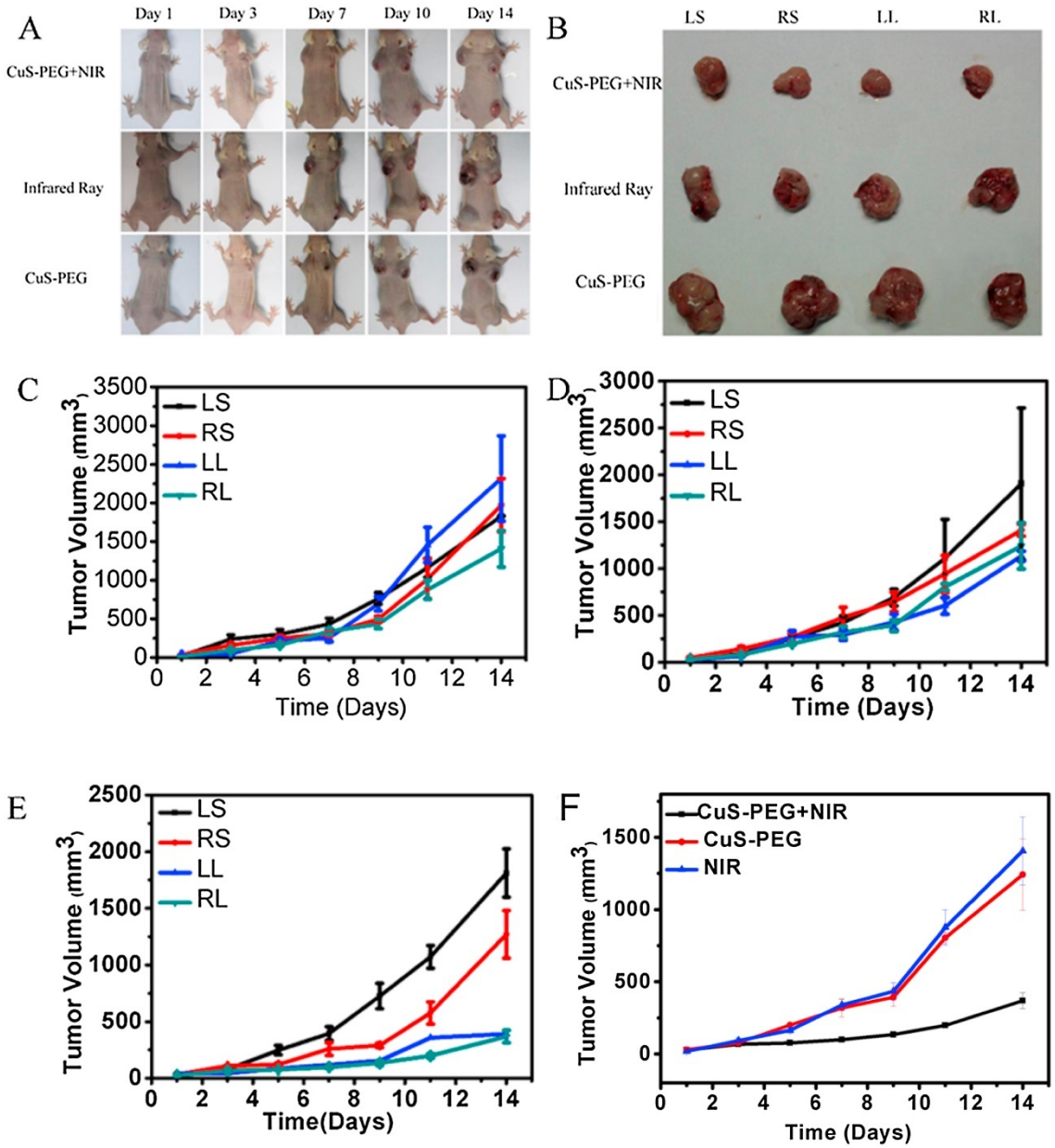

Figure 5 - Evaluation of the antitumoral capacity of Cus-PEG nanoparticles exposed to NIR. Photos of the tumor-bearing mice at 1,3,7,10, and 14 days (A) and SPC-A-1 tumors at day 14 (B) after the treatment of the nanomaterials. Tumor growth curves in the control group; 0 μL CuS-PEG in LS, 30 μL CuS-PEG in the RS, 50 μL of CuS-PEG in the LL, and 100 μL CuS-PEG in the RL (C). Tumor growth curves in the NIR – irradiated group; 0 μL NS in the LS, 30 μL NS in the RS, 50 μL NS in the LL, and 100 μL NS CuS-PEG in the RL (D). Tumor growth curves in the CuS-PEG + NIR group, 100 μL NS in the LS, 30 μL CuS-PEG in the RS, 50 μL CuS-PEG in the LL, and 100 μL CuS-PEG in the RL (E). Tumor growth volume curve comparison for 100 μL (30 μg mL^{-1}) CuS-PEG +NIR in the RL; 100 μL (30 μg mL^{-1}) CuS-PEG in the RL, and 100 μL NS in the RL (F). LS – left shoulder administration; RS – right shoulder administration; LL – left leg administration; RL – right leg administration; NS – normal saline solution. Reprinted with permission from [156]. Copyright (2017) Elsevier.

Regarding gold-based nanoparticles, to this date, two promising nanomedicines are currently in clinical trials [172]. AuroLase® uses the particles denominated as AuroShell®, a PEGylated silica-gold nanoshell with ≈150 nm in size, for the laser-activated thermal ablation of solid tumors, metastatic lung tumors, and cancer prostatic tissue [172, 176]. In the clinical trial (ClinicalTrials.gov Identifier: NCT01679470), a

single dose of AuroShell® was administered to promote the ablation of primary and/or metastatic lung tumors, still, to this date, no results were posted [177]. There is a second clinical trial (ClinicalTrials.gov Identifier: NCT00848042) involving the utilization of this nanomedicine for the treatment of patients with refractory and/or recurrent head and neck tumors, the patients were subjected to one or more doses of laser irradiation (808 nm) [76, 79]. The participants were divided into three groups: i) 5 participants, Auroshell® dose 4.5 mL kg^{-1}, laser potency 3.5 W; ii) 5 participants, Auroshell® dose 7.5 mL kg^{-1}, laser potency 4.5 W; iii) 1 participant, Auroshell® dose 7.5 mL kg^{-1}, laser potency 5 W. However, no data was published to assess the effect on the targeted tumors. In a more recent clinical trial (ClinicalTrials.gov Identifier: NCT02680535), the Auroshell® nanoparticles were tested in combination with the MRI/Ultrasound fusion technology to promote the focal ablation of neoplastic prostate tissue. The extension of this clinical trial is still active (ClinicalTrials.gov Identifier: NCT04240639), however, no data was found describing the evolution of the targeted tumors. The NU-0129® is another gold-based nanomedicine under clinical trial (ClinicalTrials.gov Identifier: NCT03020017). This nanoparticle is formed by a spherical gold nanoparticle conjugated with siRNA oligonucleotides for targeting BCL2L12 oncogene in glioblastoma multiforme or gliosarcoma treatment applications [172, 178]. The early results showed that the NU-0129® nanoparticles can cross the blood-brain barrier without unexpected adverse effects, still pending the data about the antitumoral efficacy [179].

Table 1 - Gold-based metallic-polymer nanoconjugates/nanohybrids, their physicochemical properties, and therapeutic applications (N.D.—non disclosed, N.A.—not applicable).

Metal	Morphology	Modification	Size (nm)	Surface Charge (mV)	Loading	*In Vitro*	*In Vivo*	Application	Ref.
Gold	Rods	UCST polymer (P(AAm-co-AN)-DDAT), metalloproteinase 2 (MMP-2)-sensitive peptides	Length ≈48.04; Width ≈12.08	N.D.	Doxorubicin (DOX)	HepG2 cells	HepG2 tumor-bearing mice	PTT (λex = 808 nm) and chemotherapy	[79]
		Mesoporous silica; D-α-Tocopherol polyethylene glycol 1000 succinate (TPGS), and Hyaluronic acid (HA)	Length ≈85; Width ≈64	−3 ± 5 and −10 ± 4 for TPGS/HA ratios of 1:1 and 4:1, respectively	N.A.	HeLa cells	N.A.	PTT (λex = 780 nm)	[132]
		Mesoporous silica, HA, and polyethyleneimine (PEI)	Length: 88 ± 5; Width: 63 ± 5;	−10 ± 2	Acridine Orange (AO)	HeLa cells	N.A.	PTT (λex = 750 nm) and chemotherapy	[180]
	Spheres	Poly(ethylene glycol) (PEG) and Lactofferin (LF)	5	N.D.	N.A.	Caco-2, U87MG cells	GBM tumor-bearing mice	PTT (λex = 532 nm)	[100]
	Stars	Polydopamine (PDA) and Folic acid (FA)	149 ± 3	−19 ± 2.7	DOX	MCF-7, MCF-7/ADR, NIH/3T3, and HaCaT cells	MCF-7/ADR bearing mice	PTT (λex ≈ 800 nm) and chemotherapy	[102]
		Dendritic polyglicerol (dPG) and HA	68.1	13.9	Retinoic acid (RA)	MDA-MB-231 cells	4T1 tumor-bearing mice	PTT (λex ≈ 800 nm) and chemotherapy	[181]
		PEG and CD133 antibody	≈120	−22.47	IR780/DTX	PC3 cells	PC3 tumor-bearing mice	PTT (λex = 810 nm), PDT, and chemotherapy	[182]
	Cages	Poly (acrylic acid) (p_A) or Poly(NIPAM-co-AM) (p_N)	for p_A(Au) ≈130; N.D. for p_N(Au)	≈−4 for p_A(Au) formulation at pH 7.4;	p_A(Au)-loaded with Erl and p_N(Au)	A431 or MCF-7 cells	A431 or MCF-7 tumor-	PTT (λex ≈ 800 nm for both formulations) and chemotherapy	[114]

			N.D. for p_N (Au) formulation	loaded with DOX		bearing mice		
	PVP, PEG, and anti-heat shock protein (HSP) monoclonal antibody	61.2 ± 4.85	−8.2 ± 1.25	N.A.	4T1	4T1 tumor-bearing mice	PTT (λex ≈ 808 nm)	[183]

Abbreviations—PDT: Photodynamic Therapy; PTT: Photothermal Therapy.

Table 2 - Iron-based metallic-polymer nanoconjugates/nanohybrids, their physicochemical properties, and therapeutic applications (N.D.—non disclosed, N.A.—not applicable).

Metal	Morphology	Modification	Size (nm)	Surface Charge (mV)	Loading	Longitudinal/Transverse Proton Relaxivity	*In Vitro*	*In Vivo*	Applications	Ref.
Iron	Ring	GO (graphene oxide) and CREKA (Cys-Arg-Glu-Lys-Ala)	223.3	22 ± 0.4	N.A.	N.D.	4T1 cells	4T1 tumor-bearing mice	MTD and MTT	[52]
	Spheres	HA conjugated with dopamine (HA-DA)	60.7	−16	N.A.	$r1$: 41.3 mM^{-1}	A549, HepG2, CT26, B16F10, and 4T1 cells	4T1, B16F10, and CT26 tumor-bearing mice	MRI	[145]
		PLGA, silica, Polyaniline (PANI), and R8-RGD	206	22.8	Cisplatin	$r2$: 258,5 mM^{-1} s^{-1}	A549 cells	A549 tumor-bearing mice	PTT (Strong Absorption in NIR region), MRI, and chemotherapy	[146]
		PEG, RGD, D-Glucosamine	32.31 ± 0.71	−30.2 ± 0.76	N.A.	$r2$: 554 mM^{-1} s^{-1}	4T1 cells	4T1 tumor-bearing mice	MRI and hyperthermia	[147]
		PEI, PLGA, and HA	159.5 ± 2.3	−9.1	Olaparib (Olb)	Saturation magnetizations: 21.08 emu g^{-1}	MDA-MB-231 cells	MDA-MB-231 tumor-bearing mice	RMF and chemotherapy	[184]
		PLGA, gold shell, and Herceptin	285.7 ± 81.4	N.D.	DOX	$r2$: 345.31 ± 23.06 mM^{-1} s^{-1}	BT474, MCF, and BT474/Adr cells	BT474 tumor-bearing mice	MRI, PTT (λex ≈ 750–800 nm), and chemotherapy	[185]
		AS1411 and PLGA	201.87 ± 1.60	−10.67 ± 0.25	N.A.	N.D.	MCF-7 cells	MCF-7 tumor-bearing mice	PA/US imaging and PTT (λex = 635 nm),	[186]
		HA-SS-PLA	≈11	N.D.	PTX	N.D.	HeLa cells	HeLa tumor-bearing mice	Chemotherapy	[187]
	Sheets	PDA (polydopamine), and rGO (reduced graphene oxide)	251	−27.5	N.A.	N.D.	MCF-7 cells	N.A.	MRI, PTT (Strong Absorption in NIR region), and PDT	[188]

Abbreviations—MRI: Magnetic Resonance Imaging; MTD: Magnetothermodynamic Therapy; MTT: Magnetothermal Therapy; PA: Photoacoustic Imaging; PDT: Photodynamic Therapy; PTT: Photothermal Therapy; RMF: Rotating Magnetic Field Therapy; US: Ultrasound Imaging.

Table 3 - Copper-based metallic-polymer nanoconjugates/nanohybrids, their physicochemical properties, and therapeutic applications (N.D.—non disclosed, N.A.—not applicable).

Metal	Morphology	Modification	Size (nm)	Surface Charge (mV)	Loading	*In Vitro*	*In Vivo*	Applications	Ref.
Copper	Spheres	Lanthanide-doped nanoparticles and PEG	45	N.D.	N.A.	HeLa cells	Cervical cancer tumor xenograft	NIR-II luminescence imaging/CT/MRI, CDT, and PDT	[189]
		p-(OEOMA-co-MEMA)	285	−17.2	TAPP	CT26 cells	CT26 tumor-bearing mice	PA/PI, PTT (Band from visible to NIR), PDT, and SDT	[190]
		DSPE-PEG modified with Lanreotide	186.1 ± 5.2	−16.4 ± 0.1	Docetaxel	PC-3 cells	PC-3 tumor-bearing mice	PA, PI, PTT (Band between 700 and 1000 nm), PDT, and chemotherapy	[191]
		PLGA, PDA, and PEG	288 (Higher MW-PLGA); 257 (Lower MW-PLGA)	−18.7 (Higher MW-PLGA); −22.2 (Lower MW-PLGA)	N.A.	Cal-33 cells	N.A.	MRI, PTT (N.D.), and chemotherapy	[192]
		HA/PEI	330.7	16.9	Disulfiram	Eca109	Eca109 tumor-bearing mice	Chemotherapy and FL	[193]
		PEG-NH_2 and PCL-SS-P(DPA/GMA/MP)	151.5 ± 2.2	−17.1 ± 1.7	Dox	L929 and 4T1	4T1 tumor-bearing mice	PTT (Strong absorption in the NIR region), and chemotherapy	[194]
		HA and PDA	106	−19.43	Dox	HeLa and 4T1	4T1 tumor-bearing mice	PA, PTT (N.D), CDT, and chemotherapy	[195]
	Framework	Pluronic F127	186.4 ± 16.7	−1.2 ± 0.1	O_2	4T1 and HeLa cells	4T1 tumor-bearing mice	PDT (Band from visibile to NIR)	[196]
	Cubes	BSA and PEG-FA	60	N.A.	N.A.	HepG2 cells	N.A.	PTT (Band from visible to NIR) and chemotherapy	[197]

Abbreviations— CT: Computed Tomography; PA: Photoacoustic Imaging; PDT; Photodynamic Therapy; PTT: Photothermal Therapy; SDT: Sonodynamic Therapy.

Table 4 - Summary of the Platinum/Silver/Zinc-based metallic-polymer nanoconjugates/nanohybrids, their physicochemical properties, and therapeutic applications (N.D.—non disclosed, N.A.—not applicable).

Metal	Morphology	Modification	Size (nm)	Surface Charge (mV)	Loading	*In Vitro*	*In Vivo*	Applications	Ref.
Platinum	Spheres	PDA and Folate	≈100	N.A.	Indocyanine Green (ICG)	MCF-7	Breast cancer tumor xenograft	PA, FL, PTT (λex≈700–800 nm), and PDT	[164]
		PEG	120	−14.6	DOX	4T1	4T1 tumor-bearing mice	EDT and chemotherapy	[166]
		HA	38 ± 6	−31 ±1	N.A.	MDA-MB-231 (CD44+) and PC9 (CD44-)	MDA-MB-231 tumor-bearing mice	PI and PTT (N.D.)	[167]
		PEG	119.7	−1.6 ± 0.4	Cisplatin and IR780	4T1	4T1 tumor-bearing mice/Hepatocellular Carcinoma Patient Derived Xenograft	PI, FL, PTT (λex = 780 nm), and chemotherapy	[198]
Silver	Globular irregular shape	BSA and PEG	131.5 ± 2.7	−34.68 ±0.6	ICG	B16F10 cells	B16F10 tumor-bearing mice	PTT (λex≈790 nm)	[171]
	Spheres	Polythiourea and PEG	25–30	N.D.	N.A.	A549	A549 tumor-bearing mice	FL	[199]
		HA	104 ± 6.2	−30	N.A.	4T1	4T1 tumor-bearing mice	FL and RT	[200]
	Dots	FA modified DSPE-PEG_{2000}	200	−30.84	N.A.	HeLa and A549 cells	HeLa tumor-bearing mice	FL/PA imaging and PTT (Strong absorption in the visible and NIR region)	[201]
Zinc	Spheres	PVP40	≈5	−3.6	N.A.	SW480 and HEK293T cells	SW480 tumor-bearing mice	PDT (N.D.)	[161]
		PDA	≈175	−21.7	DOX and DNAzyme	A549 cells	A549 tumor-bearing mice	FL, PI, GT, PTT (N.D.), and chemotherapy	[202]
		PEG and RGD	112.0 ± 3.2	−14.6 ± 5.2	PTX	4T1 cells	4T1 tumor-bearing mice	MRI, NIRFI, and chemotherapy	[203]
		PEG and PLGA	PLGA-ZnNPc-NP = 141; PLGA-ZnPc-NPs = 152	PLGA-ZnNPc-NPs = 4.8; PLGA-ZnPc-NPs = 5.1	N.A.	MCF-7 cells	DMBA-induced breast cancer-bearing mice	FL and PDT (N.D.)	[204]

Abbreviations— – CDT: Chemodynamic Therapy; EDT: Electrodynamic Therapy; FL: Fluorescence Imaging; GT: Gene Therapy; MRI: Magnetic Resonance Imaging; NIRFI: Near Infrared Fluorescence Imaging; PA: Photoacoustic Imaging; PDT: Photodynamic Therapy; PI: Photothermal Imaging; PTT: Photothermal Therapy; RT: Radiotherapy. Therapy.

Table 5 - Summary of clinical trials comprising metallic-polymer nanoconjugates/nanohybrids (N.A.—not applicable).

Name	Description	Application	Administration Route	Type of Cancer	Clinical Trials Identifier (Phase)	Results	Ref.
Magnablate®	Iron oxide nanoparticles	Magnetic Hyperthermia	Intratumoral	Prostate Cancer	NCT02033447 (Early Phase I): Completed	No results yet available	[175]
Nanotherm®	Iron oxide nanoparticles	Magnetic Hyperthermia	Intratumoral	Brain tumor	Approved by the EMA in 2010		[83]
			Intratumoral	Prostate Carcinoma	NCT05010759: Still recruiting (Phase not applicable)	No results yet available	N.A.
AuroLase®	PEGylated silica-gold nanoshell (AuroShell®)	Laser-activated termal ablation	Intravenous	Metastic lung tumors	NCT01679470: Phase not applicable	No results yet available	[177]
				Refractory and/or recurrent head and neck tumors	NCT00848042: Phase not applicable	No results yet available	N.A.
		Laser-activated termal ablation combined with MRI/US fusion technology for focal ablation		Neoplastic Prostate tissue	NCT02680535 and NCT04240639 (extension of the previous): Phase not applicable	No results yet available	N.A.
NU-0129®	Spherical gold nanoparticle conjugated with siRNA oligonucleotides	Targeting BCL2L12 oncogene	Intravenous	Glioblastoma multiforme or Gliosarcoma Treatment	NCT03020017: Completed	No results provide about the antitumor efficacy	[179]

Abbreviations— EMA: European Medicines Agency; MRI: Magnetic Resonance Imaging; US: Ultrasound Imaging.

Aims

The main objective of this dissertation was to design and develop a novel synthesis approach to produce gold-polymer nanohybrids for application in cancer therapy. For that purpose, alginic acid was selected due to its biocompatibility, hydrophilicity, and negative charge that was explored to guide the nanomaterials formation, *i.e.*, the gold reduction.

The specific goals of the dissertation work were:

- Synthesis of a gold-alginic acid nanohybrids (Au-Alg-NH);
- Characterization of the Au-Alg-NH physicochemical properties;
- Evaluation of the photothermal capacity of Au-Alg-NH;
- Characterization of the Au-Alg-NH biocompatibility;
- Evaluation of the Au-Alg-NH cellular uptake and cytotoxic activity using a breast cancer cell *in vitro* model.

Chapter 2

Experimental Section

2. Experimental Section

2.1 Materials

Hydrogen tetrachloroaurate (III) hydrate ($HAuCl_4$) and Calcium chloride ($CaCl_2$) were acquired from Alfa Aesar (Karlsruhe, Germany). Dulbecco's Modified Eagle medium-high glucose (DMEM-HG), Dulbecco's Modified Eagle Medium/ Nutrient Mixture F-12 (DMEM/F-12), Phosphate-buffered saline solution (PBS), Fluorescein 5-isothiocyanate (FITC), Ethanol, Trypsin, Resazurin, Paraformaldehyde (PFA) and Alginic acid sodium salt (from brown algae) were bought from Sigma-Aldrich (Sintra, Portugal). Fetal bovine serum (FBS) was purchased from Biochrom Ag (Berlin, Germany) and L-ascorbic acid was acquired from Fischer Scientific (Oeiras, Portugal). Human negroid cervix epithelioid carcinoma (HeLa) (ATCCs CCL-2TM) and Michigan Cancer Foundation-7 (MCF-7) were acquired by ATCC (Middlesex, UK). Normal Human Dermal Fibroblast (FibH) cells were obtained from PromoCell(Lab-clinics,S.A.,Barcelona,Spain). Cell culture plates and T-flasks were obtained from Thermo Fischer Scientific (Porto, Portugal). Cell imaging plates were bought from Ibid GmbH (Munich, Germany). Wheat germ agglutinin conjugate Alexa 594® (WGA-Alexa Fluor 594®) and Hoechst 33342® were acquired from Invitrogen (Carlsbad). Double ionized and filtered water was obtained by using a Milli-Q Advantage A10 Ultrapure Water Purification System (ddH_2O: 0.22 μm filtered; 18.2 MΩ cm^{-1} at 25 ºC).

2.2. Methods

2.2.1. *Green* synthesis of gold-polymer nanohybrids

Gold-alginic acid nanohybrids (Au-Alg-NH) were synthesized by adapting a method previously described in the literature [45]. Briefly, 1.125 mL of $CaCl_2$ (2.0 mg mL^{-1}) were added to a solution that contained 10 mL of alginic acid (0.3 mg mL^{-1}) and 0.375 mL of $HAuCl_4$ (0.05 M), and left to react under magnetic stirring for 30 min at room temperature. Then, the obtained solution was centrifuged (18000 g, for 20 min, at 25 ºC) and the recovered supernatant was resuspended in ddH_2O. Subsequently, L-ascorbic acid (0.08 M) was dissolved in 1 mL of ddH_2O and added to the previous solution, and left to react for 1 h under magnetic stirring. The obtained Au-Alg-NH were washed with ddH_2O and recovered by centrifugation (3 cycles, 9000 g for 20 min at 4 ºC) to remove the excess of polymer.

2.2.2. Characterization of Au-Alg-NH' physicochemical properties

2.2.2.1. Morphological characterization

The morphology of the Au-Alg-NH was assessed by Transmission electron microscopy (TEM; TECNAI G2 20 S-TWIN, EI Company, Amsterdam, The Netherlands). For that purpose, the nanoparticles were placed on formvar-coated copper grids and allowed to dry at room temperature. The TEM images were obtained at an accelerating voltage of 200 kV.

2.2.2.2. Size and zeta potential analysis

The nanoparticles' size and surface charge were determined by using a Zetasizer Nano ZS equipment (Malvern Instruments, Worcestershire, United Kingdom). In all measurements, the nanoparticles were resuspended in ddH_2O and the data was collected in a disposable capillary cell at 25 ºC.

2.2.2.3. Ultraviolet-visible spectroscopy analysis

The success of the Au-Alg-NH synthesis and their NIR absorption capacity was evaluated by the acquisition of the nanomaterials' UV-Vis-NIR absorption spectrum (Thermo Scientific EvolutionTM201 Bio UV-vis Spectrophotometer, Thermo Fisher Scientific Inc., USA) at a scanning rate of 300 nm min^{-1}, with a wavelength range between 300 and 1100 nm.

2.2.2.4. *In vitro* photothermal measurements

The evaluation of the Au-Alg-NH *in vitro* photothermal capacity was performed as previously reported in the literature [39]. For that purpose, Au-Alg-NH at 3 different concentrations (100, 150, and 200 µg mL^{-1}) were irradiated with a NIR laser (808 nm, 1.7 W cm^{-2}). The temperature variation was recorded at different time points (from 1 up to 10 min) using a thermocouple sensor with an accuracy of 0.1 ºC. The control group was composed by ddH_2O exposed to NIR light. Additionally, the photothermal stability of Au-Alg-NH after multiple irradiations was also measured at the same timepoints (from 1 up to 10 min).

The photothermal conversion efficiency of Au-Alg-NH was calculated through equation 1:

$$\eta = \frac{hS(Tmax - Tsol.amb) - Qdis}{I(1 - 10^{-A808})} \quad \text{(Equation 1)}$$

, where h is the heat transfer coefficient, S is the surface container area, $Tmax$ is the highest temperature recorded by the samples, $Tsol.amb$ is the room temperature, I is the NIR laser intensity, A_{808} corresponds to the absorbance of the nanoparticles at 808 nm [205]. The value of Qdis and hS are obtained using the following equations:

$$Qdis = \frac{1000 * \mathrm{mC} * \Delta\mathrm{T}}{t} \text{ (Equation 2)}$$

$$\mathrm{hS} = \frac{\mathrm{m.C}}{\tau\mathrm{s}} \text{ (Equation 3)}$$

, where m is the water mass (0.2 g), C is the specific heat capacity of water (4.2 J g^{-1} C^{-1}), ΔT is the temperature increase value, t is the samples' irradiation time (600 s) and τs is the sample system time constant, which is calculated through equation 3:

$$\tau\mathrm{s} = \frac{\mathrm{t}}{\ln(\theta)} \text{ (Equation 4)}$$

, where θ is determined through equation 4:

$$\theta = \frac{\mathrm{Tamb} - \mathrm{Tsol.amb}}{\mathrm{Tmax} - \mathrm{Tsol.amb}} \text{ (Equation 5)}$$

, where $Tamb$ corresponds to the room temperature (22.1 ºC).

2.2.2.5. Thermogravimetric analyisis

The polymer and gold content of Au-Alg-NH was determined by thermogravimetric analysis (TGA). Alginic acid nanoparticles crosslinked with $CaCl_2$ and each raw material were also analyzed for comparison purposes. Briefly, all samples were subjected to increasing temperatures at a rate of 10 ºC min^{-1} until reaching 600 ºC. The samples' weight loss was recorded over time under an inert atmosphere using a SDT Q600 equipment (TA Instruments, USA).

2.2.3 Cytocompatibility assay

The cytocompatibility of Au-Alg-NH was evaluated through a resazurin-based assay towards MCF-7 and FibH cells at three-time points [206]. This method is based on the intracellular reduction of resazurin (non-fluorescent reagent) to a fluorescent pink-reddish soluble resorufin. For that purpose, both cell lines were seeded at a density of 10000 cells/ well into 96-well flat-bottom culture plates, and cultured with 100 µL of

DMEM/F-12 (with 10% FBS (v v^{-1}) and 1% penicillin/streptomycin (v v^{-1})) for 48 h in an incubator with a humidified atmosphere (37 ºC, 5% CO_2). After that time, the culture medium was replaced, and the cells were incubated with increasing concentrations of Au-Alg-NH (25 to 200 µg mL^{-1}) for 24, 48, and 72 h. Posteriorly, the culture medium was replaced with 110 µL of 10% (v v^{-1}) resazurin in the dark at 37 ºC for 4 h. Then, the cell viability was determined by measuring the fluorescence of the produced resorufin using a spectrofluorometer (Spectramax Gemini XS, Molecular Devices LCC, USA) at an excitation/ emission wavelength of λ_{ex}=560 nm and λ_{em}=590 nm. Cells only incubated with the culture medium were used as a negative control (K^-). Cells incubated with ethanol (99.9%) were used as the positive control (K^+).

2.2.4. Evaluation of cellular uptake

The uptake of Au-Alg-NH by FibH, MCF-7, and HeLa cells was assessed by fluorescence spectroscopy and confocal microscopy, through methods already described in the literature [207, 208]. Briefly, each cell line was seeded in 96-well flat-bottom culture plates (12000 cells/ well, 100 µL of DMEM-HG or DMEM-F12 medium) in a humidified atmosphere (37 ºC, 5% CO_2). After 48 h, the culture media was removed and cells were incubated with FITC-stained Au-Alg-NH (200 µg mL^{-1}) for 2 and 4 h. Thereafter, cells were washed with ice-cold Krebs Ringer Buffer (KRB) and lysed with Triton X-100 (1% in KRB for 30 min, under stirring at room temperature). Cells only incubated with KRB were used as control. The FITC-stained nanoparticles' internalization was quantified by measuring the FITC fluorescence (λ_{ex}=480 nm and λ_{em}=570 nm) using a spectrofluorometer (Spectramax Gemini XS, Molecular Devices LCC, USA).

Confocal laser scanning microscopy (CLSM) experiments were further performed to confirm the uptake results, following a method previously described in the literature [207]. Briefly, MCF-7 cells were seeded on µ-Slide 8 well Ibidi imaging plates (20000 cells/well, 200 µL of DMEM-F12 medium) at 37 ºC in a humified atmosphere (5% CO_2) for 48 h. Then, the culture medium was removed and FITC-stained nanoparticles (200 µg mL^{-1}) were incubated for 2 and 4 h. After that period, cells were washed with PBS and fixed with PFA 4% (w v^{-1}) for 10 min at room temperature and washed again with PBS. Finally, the cells were treated with WGA-Alexa Fluor 594® (30 min followed by several washes with PBS) and Hoechst 33342® (20 min followed by several washes with PBS), for the cytoplasm and nucleus staining, respectively. The CLSM images were acquired using a Zeiss LSM 710 microscope (Carl Zeiss, Germany), with posterior image analysis and tridimensional reconstruction in Zeiss Zen 2010 software.

2.2.5. Characterization of nanoparticles *in vitro* phototherapeutic effect

The NIR-triggered cytotoxic effect of the Au-Alg-NH was evaluated on MCF-7 cells through the resazurin assay [206] upon 3 irradiation cycles with a NIR laser. Briefly, MCF-7 cells were seeded in 96-well flat-bottom plates (10000 cells/well, 100 µL of DMEM/F-12) at 37 ºC in a humified atmosphere (5% CO_2) for 48 h. Afterward, the cultured medium was removed, and cells were incubated with different concentrations of Au-Alg-NH (150 or 200 µg mL^{-1}). After 12 h of incubation, cells were submitted to 3 irradiation cycles of NIR laser (808 nm, 1.7 W cm^{-2} for 10 min). Non-irradiated cells were used as control (KNIR). After the 3 irradiation cycles, the cells' viability was assessed using the resazurin method as described above. Cells only incubated with the culture medium were used as a negative control (K^-). Cells incubated with ethanol (99.9%) were used as the positive control (K^+).

2.2.6. Statistical analysis

All data are presented as the mean ± standard deviation (s.d.). One-way analysis of variance (ANOVA) with the student-Newman Keuls test was used to compare different groups. A p-value < 0.05 was considered statistically significant. The statistical analysis was performed in GraphPad Prism v.7.01 software (Trial version, GraphPad Software, CA, USA).

Chapter 3

Results and Discussion

3. Results and Discussion

3.1. Production and characterization of Au-Alg-NH

The main goal of this dissertation work plan was to develop a novel synthesis approach to produce Au-Alg-NH for application in cancer photothermal therapy (Figure 6). Gold is one of the most explored materials for producing metallic nanoparticles due to their promising optical properties (*e.g.* localized surface plasmon resonance), light-to-heat conversion efficiency, and facile surface functionalization. The alginic acid was selected due to its biocompatibility, hydrophilicity, and negative charge that was explored to guide the nanomaterials formation [209]. For that purpose, the production of Au-Alg-NH was achieved in a one-pot synthesis by promoting gold reduction and nucleation in the presence of alginic acid and $CaCl_2$.

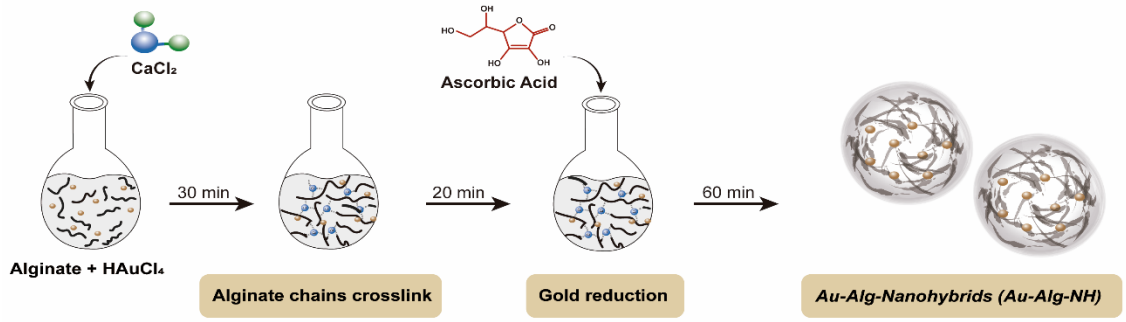

Figure 6 – Schematic representation of the one-pot Au-Alg-NH synthesis.

The successful synthesis of the gold-alginic acid nanohybrids was confirmed by TEM (Figure 7). The analysis of TEM images demonstrates that the Au-Alg-NH acquire an anisotropic spike-like shape, resembling the gold nanostars, with gold conjugation throughout the alginic acid in nanohybrids, with the particles [210]. The nanoparticles present an average size of 153 nm, ImageJ measurements based on TEM images (Figure 7). Moreover, the DLS analysis showed that the Au-Alg-NH have a homogenous distribution with a hydrodynamic size averaging 305 nm (Figure 8A). This size value is still within the range suitable for intravenous administration, circulation in the human body, and accumulation in the tumor tissue [52, 115, 185, 192, 193]. The difference in TEM and DLS measurements can be attributed to the sample state in each technique, dried preparation for TEM analysis commonly results in smaller nanoparticle sizes. Additionally, the surface charge measurements showed that the Au-Alg-NH have a negative value, -25 mV ± 4.5 mV, which is in accordance with the negative charge of alginic acid. Despite not being within the neutral range of surface charge, it is worth

noticing that the negative charges often translate into lower phagocytic uptake thereby contributing to the increase of the nanoparticles' blood circulation time [36].

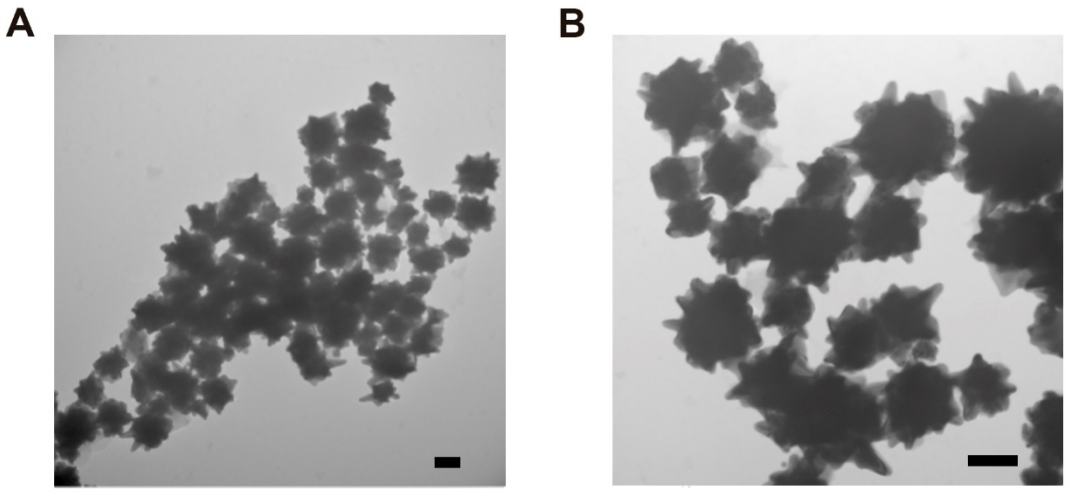

Figure 7 - TEM images of Au-Alg-NH at different ampliations. Scale bar: 100 nm.

The colloidal stability of the Au-Alg-NH was evaluated during 3 weeks of storage, resuspended in ddH_2O at room temperature (Figure 8B). The obtained results show that the nanoparticles' size remained relatively constant during the experience, with less than 10% of variation after 3 weeks. Moreover, a similar result was observed in the measurement of the nanoparticles' surface charge (Figure 9A). These results may be attributed to the negative charge of the nanoparticles that allows the establishment of electrostatic repulsion interactions, preventing the aggregation of Au-Alg-NH [211].

Furthermore, the thermal stability of the Au-Alg-NH by thermogravimetric analysis, monitoring the weight changes in response to the temperature increase up to 600 ºC (Figure 9B). The obtained curves show that Au-Alg-NH remain stable during the experiment, being only detected a loss of 2% of the total weight. Such data is indicative that the *in situ* gold reduction increases the nanoparticles' thermal stability since the alginic acid control group showed a loss of 64% of the total mass, as a result of polymer pyrolysis.

3.2. *In vitro* evaluation of the Au-Alg-NH photothermal capacity

The potential photothermal effect of Au-Alg-NH was initially characterized by Uv-vis analysis (Figure 10B). The spectra show that an increase in the concentration of the nanoparticles, from 75 to 200 μg mL^{-1}, resulted in a higher absorbance capacity along the

spectra. The organization into gold-conjugated nanohybrids induced a redshift in the absorption peak, relative to the usual gold sphere band (between 500-550 nm) [28], leading to an absorption peak around 620 nm. Moreover, the Au-Alg-NH also showed an enhanced absorption capacity in the NIR region, which was indicative of a possible application in photothermal therapy. Furthermore, the obtained absorption spectra are similar to those reported in the literature for different gold nanostar formulations [212, 213].

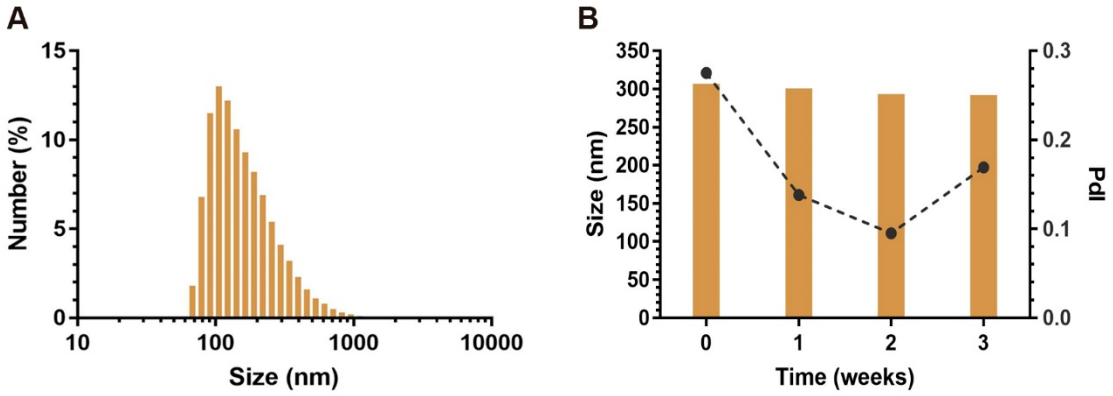

Figure 8 - Size analysis and colloidal stability of Au-Alg-NH formulation. (A) DLS size distributions of Au-Alg-NH and (B) size and Pdi variation over 3 weeks. Data are presented as mean ± s.d., n=300.

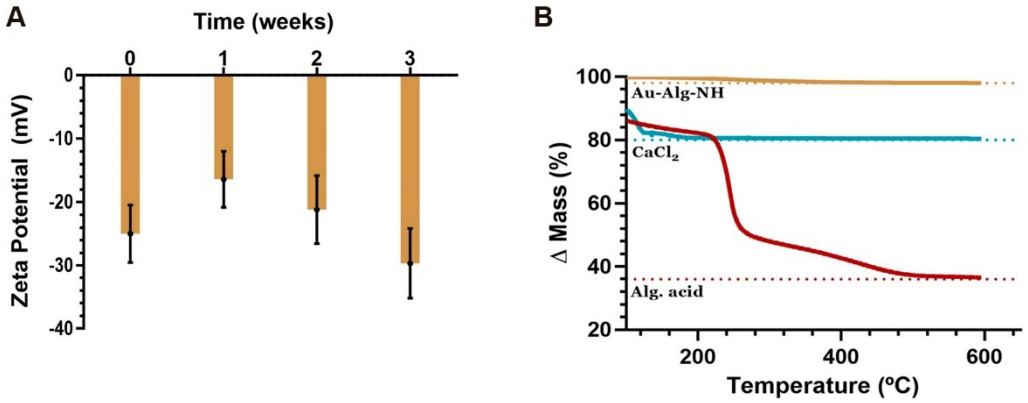

Figure 9 - Physicochemical characterization of Au-Alg-NH. (A) Surface charge variation over 3 weeks, data are presented as mean ± s.d., n=3 and (B) TGA analysis of Au-Alg-NH, CaCl2 and alginic acid.

The Au-Alg-NH' ability to transform the light energy into heat was then explored by measuring the temperature changes in response to the irradiation with a NIR laser (808 nm, 1.7 W cm^{-2}) (Figure 10A, 10 C). The temperature variation curves show that at a concentration of 200 µg mL^{-1}, the Au-Alg-NH mediated a temperature increase of 11.3 ºC, which corresponds to a photothermal conversion efficiency of 39.3%. Furthermore, to test whether the nanoparticles underwent any changes in their conformation or photothermal potential, the Au-Alg-NH were subjected to multiple irradiation cycles (Figure 10D). During the 3 irradiation cycles, the maximum temperature achieved was

slightly superior to 11 ºC, showing the photothermal stability of the Au-Alg-NH. This photothermal capacity was similar to that observed in other similar-shaped gold nanostars reported in the literature [214-216]. Nevertheless, it should be highlighted that the observed temperature variations are suitable to induce cell death by disrupting the cell membrane, causing DNA damage, and/or altering metabolic pathways.

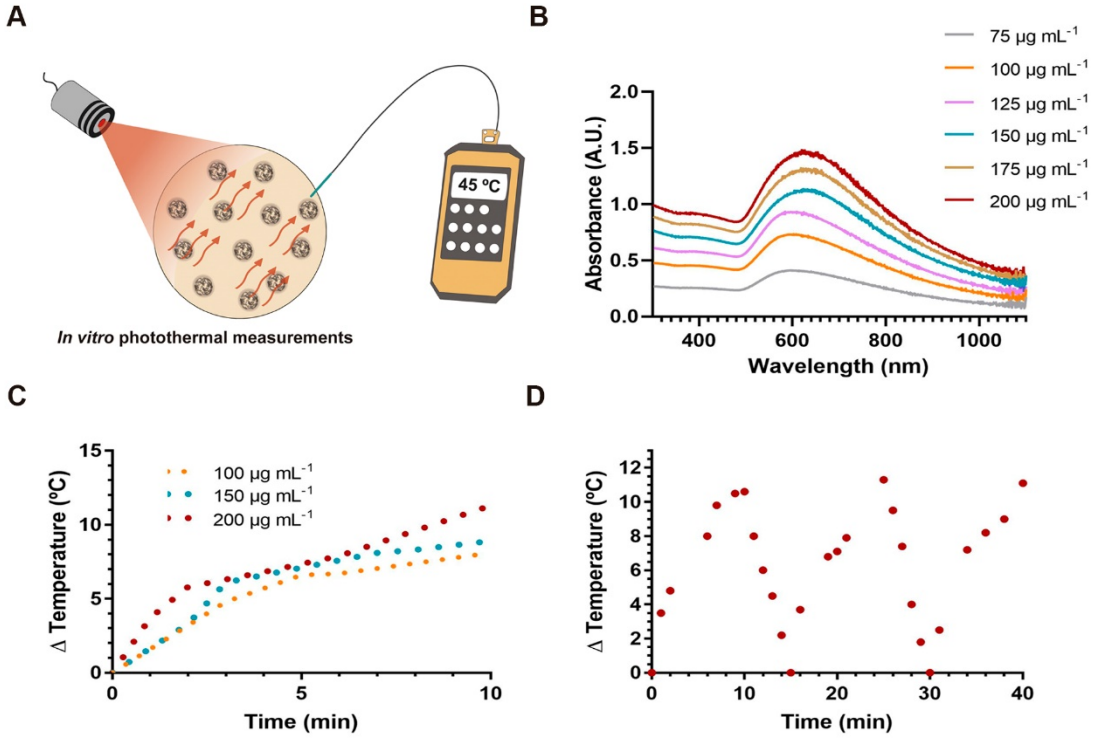

Figure 10 - Evaluation of the Au-Alg-NH photothermal capacity. (A) Schematic representation of the *in vitro* photothermal measurements. (B) UV-Vis spectra of different concentrations of Au-Alg-NH (from 75 to 200 µg mL^{-1}. (C) Temperature variation curves of Au-Alg-NH (100, 150, and 200 µg mL^{-1}) in ddH_2O, NIR laser (808 nm, 1.7 W cm^{-2}) irradiation for 10 min. (D) Temperature variation curve of Au-Alg-NH (200 µg mL^{-1}) exposed to multiple irradiation cycles. Data are presented as mean ± s.d., n=3.

3.3. Characterization of the nanoparticles' biocompatibility

The biocompatibility of nanoparticles is one of the major factors impacting their use in biomedical applications. According to the threshold presented in the ISO 10993-part V "Biological evaluation of medical devices", a material should be considered cytotoxic if occurs a reduction of cell viability by more than 30%. Therefore, cell viabilities superior to 70% will be indicative of the Au-Alg-NH' biocompatibility and safety [217]. The Au-Alg-NH' cytocompatibility was assessed both on FibH and MCF-7 cells through the metabolic-based resazurin assay. To that end, different Au-Alg-NH concentrations, ranging from 25 to 200 µg mL^{-1}, were incubated with the cells and its effect on the cells' viability was evaluated after 24, 48, and 72 h (Figure 11). The obtained results show that the cellular viabilities remain superior to the threshold of 70% even at the highest tested concentration, 200 µg mL^{-1}, and longest incubation time (*i.e.*, 72 hours). Such data attests

the Au-Alg-NH' cytocompatibility and are in accordance with the well-known biocompatibility of alginic acid and other results available in the literature for similar nanoparticle formulations.

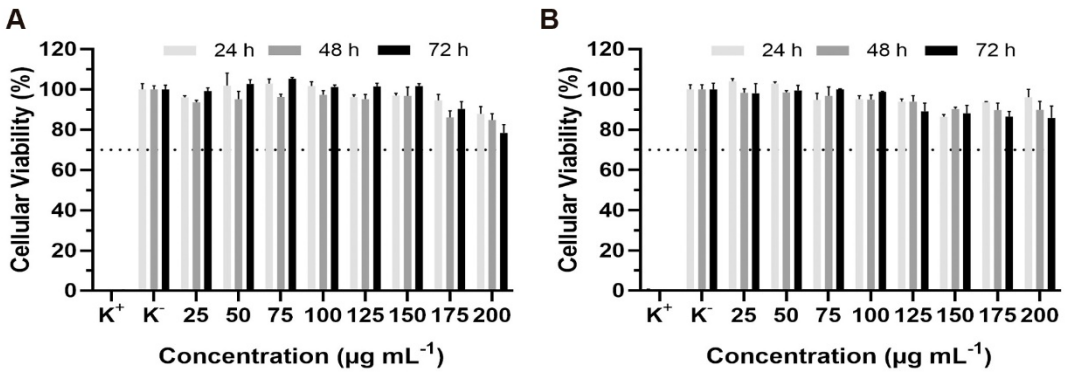

Figure 11 – Evaluation of Au-Alg-NH cytocompatibility in FibH and MCF-7 cells at 24, 48, and 72 h. (A) Cytocompatibility analysis for Au-Alg-NH in FibH cells and (B) MCF-7 cells. Positive control (K^+): cells treated with EtOH; negative control (K^-): cells without nanoparticle incubation. Data are presented as mean ± s.d.

3.4. Au-Alg-NH uptake by FibH and MCF-7 cells

After determining the nanoparticles' cytocompatibility, the Au-Alg-NH uptake was studied in FibH, MCF-7, and HeLa cells using fluorescence spectroscopy and CLSM (Figure 12). For that purpose, Au-Alg-NH were labelled with FITC to allow the tracking of the nanoparticles.

The obtained results show that despite the negative surface charge the Au-Alg-NH can be internalized by cancer cells. In fact, the fluorescence spectroscopy data indicate a superior internalization of Au-Alg-NH in HeLa and MCF-7 cancer cells. Such may be justified by the higher growth rate of cancer cells, which can facilitate the nanoparticles' uptake during the reorganization of the cytoplasmatic membrane. Moreover, the CLSM images corroborate these findings being possible to observe the presence of the Au-Alg-NH inside the MCF-7 cancer cells (Figure 12 C, 12D, white arrows). Altogether, these data demonstrate that the Au-Alg-NH can overcome the last biological barrier that the nanoparticles encounter when administered in the human body, the cancer cells membrane, and in this way result in more effective therapies.

3.5. Evaluation of the Au-Alg-NH phototherapeutic activity

The photothermal anti-cancer effect of Au-Alg-NH was evaluated in MCF-7 cells upon NIR laser irradiation (Figure 13). For that purpose, Au-Alg-NH were incubated at a concentration of 150 or 200 µg mL^{-1} with MCF-7 cells for 2 days and irradiated 3 times

with a NIR light (808 nm, 1.7 W cm^{-2}, 10 min). The obtained results indicate that an increase in the nanoparticles' concentration led to higher cell death in response to the NIR light irradiation and consequent heat generation. In fact, the Au-Alg-NH, at the concentration of 200 μg mL^{-1}, mediated the decrease in the cells' viability to values inferior to 30% (Figure 13B). These results are in agreement with other reports available in the literature for photothermal agents with similar heat generation capacity (*i.e.*, ≈ 11 ºC) [214-216]. The increase in the temperature to values superior to 45 ºC has a negative impact on the cells' functions, namely can provoke the rupture of the cell membrane, DNA damage, protein denaturation, and induce programmed cell death or cell necrosis [28, 83, 84].

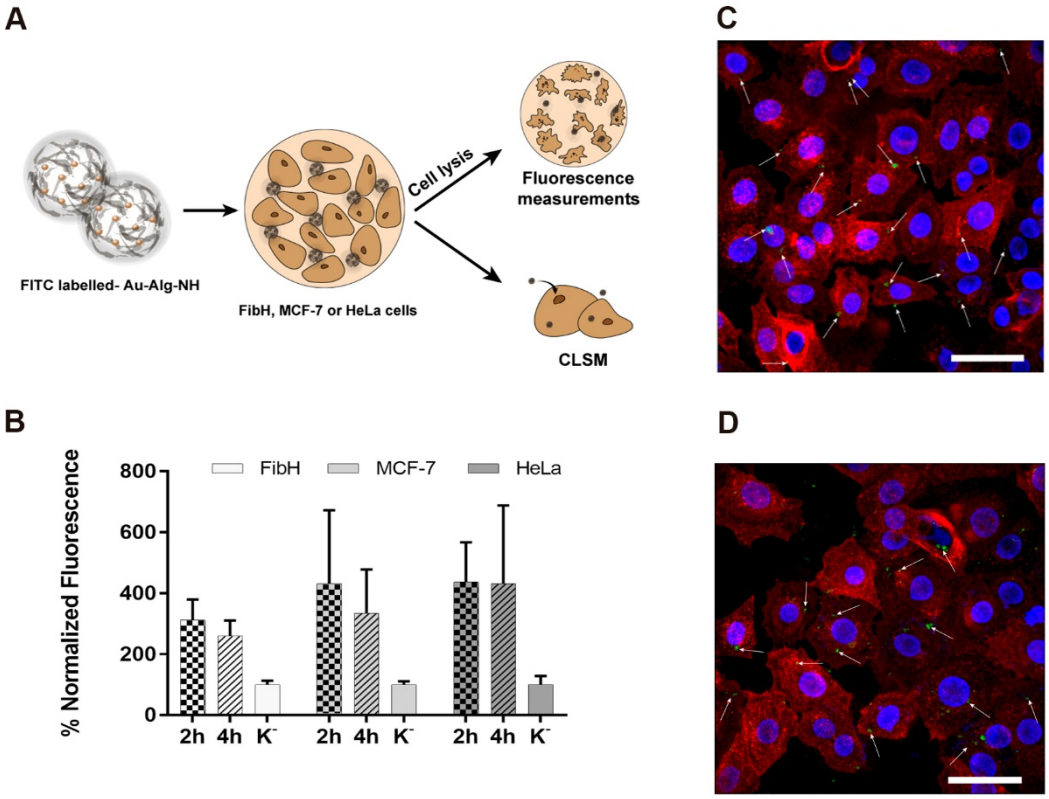

Figure 12 – Evaluation of the Au-Alg-NH uptake by FibH, MCF-7, and HeLa cells. (A) Schematic representation of the uptake experiments. (B) Fluorescence spectroscopy analysis of Au-Alg-NH uptake by FibH, MCF-7, and HeLa cells. CLSM images of FITC stained Au-Alg-NH after (C) 2 and (D) 4 h of incubation. The white arrows are pointing to internalized nanoparticles. Blue channel: Hoechst 33342® stained cell nucleus; red channel: WGA-Alexa Fuor 594® stained cell cytoplasm; green channel: FITC-labeled Au-Alg-NH.

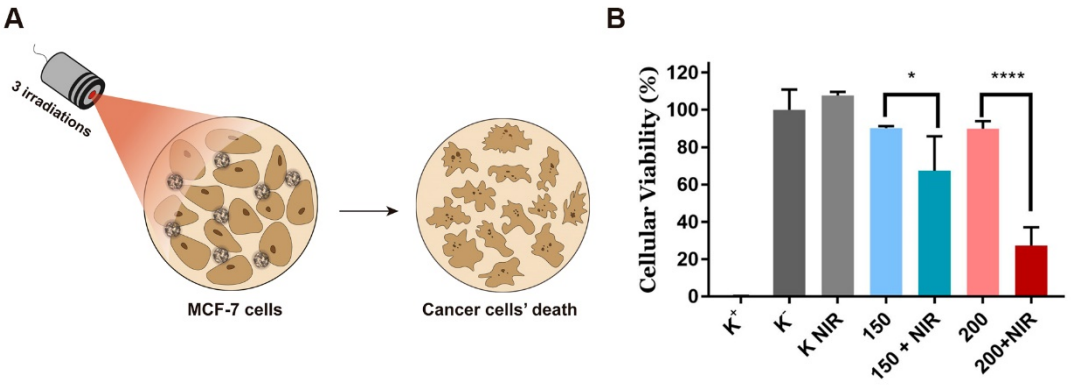

Figure 13 – Analysis of the Au-Alg-NH photothermal cytotoxic effect in MCF-7 cancer cells. (A) Schematic representation of the Au-Alg-NH cytotoxic activity upon NIR irradiation (3 cycles, 808 nm, 1.7 W cm^{-2}, 10 min) (B) Analysis of the MCF-7 cell viability in response to treatment with different nanoparticles concentration (150 and 200 μg mL^{-1}), fluorescence was normalized to the K NIR groups. K^+: cells treated with EtOH. K^-: MCF-7 cells without irradiation or nanoparticle incubation and K NIR: MCF-7 cells exposed to NIR irradiation (3 cycles, 808 nm, 1.7 W cm^{-2}, 10 min). Data are presented as mean ± s.d., *p<0.05, ****p>0.0001, n=3.

Chapter 4

Conclusion and Future Perspectives

4. Conclusion and Future Perspectives

Currently, despite continued efforts, cancer remains a major cause of death worldwide. Moreover, the currently available treatments present suboptimal efficacies and often can only delay the cancer progression. Therefore, there is an urgent demand for novel and more effective cancer therapies. In this topic, the breakthroughs of the nanotechnology field pave the way for the development of novel solutions and therapeutic approaches to cancer. Among the several nanomaterials that have been under study, the gold-based nanoparticles show the potential for developing multifunctional anticancer platforms due to their innate bioimaging capacity (*e.g.*, computed tomography contrast agent) and drug delivery/photothermal effect. However, the gold-based nanoparticles often present suboptimal toxicological profiles and colloidal stability (high interaction with blood proteins) as well as off-target interactions.

Taking this into account, this dissertation work plan aimed at designing and developing a novel synthesis approach to produce gold-alginic acid nanomaterials for application in cancer therapy. The successful synthesis of these nanohybrids materials was confirmed by TEM and DLS, with the particles showing a uniform size distribution and a spike-like shape. Additionally, the Au-Alg-NH were stable in solution for 3 weeks and could mediate a temperature increase of 11.3 ^{o}C in response to the irradiation with a NIR laser (808 nm, 1.7 W cm^{-2}, for 10 min). Preliminary *in vitro* assays indicated that the Au-Alg-NH do not induce cytotoxicity (*i.e.*, cell viability superior to 70%) even at the highest tested concentration of 200 μg mL^{-1} at 72 h of incubation and are efficiently internalized by cancer cells. Nevertheless, upon irradiation with a NIR laser (3 cycles, 808 nm, 1.7 W cm^{-2} for 10 min) the Au-Alg-NH (200 μg mL^{-1}) mediated the reduction of the MCF-7 cells' viability to ≈27%.

In the near future, the surface modification of the Au-Alg-NH with targeting moieties (*e.g.*, aptamers, folate, and RGD sequence) will be pursued to imprint in the nanoparticles an active recognition of the cancer cells. Moreover, this surface modification may also be explored to neutralize the surface charge of Au-Alg-NH. Furthermore, the loading of therapeutic molecules, such as drugs and photothermal/photodynamic agents, will also be tested to increase the therapeutic efficacy of the nanomaterials. Finally, the Au-Alg-NH therapeutic capacity will also be assessed in more complex disease models, *i.e.*, tumor spheroids, to evaluate the possibility to proceed to the *in vivo* assays. In the case of sub-optimal performances, will

be considered the re-engineering of the Au-Alg-NH, such as a decrease in the nanoparticles' size that can favor the penetration in the tumor tissue.

Chapter 5

References

5. References

1. Arneth, B., Tumor Microenvironment. *Medicina* **2020,** 56, (1), 15.
2. Sung, H.; Ferlay, J.; Siegel, R. L.; Laversanne, M.; Soerjomataram, I.; Jemal, A.; Bray, F., Global Cancer Statistics 2020: GLOBOCAN Estimates of Incidence and Mortality Worldwide for 36 Cancers in 185 Countries. *CA: A Cancer Journal for Clinicians* **2021,** 71, (3), 209-249.
3. Miranda N, Gonçalves MB, Andrade C, Santos G. Programa Nacional para as Doenças Oncológicas. Direção-Geral da Saúde 2017.
4. Perrino, M.; Cooke-Barber, J.; Dasgupta, R.; Geller, J. I., Genetic predisposition to cancer: Surveillance and intervention. *Seminars in Pediatric Surgery* **2019,** 28, (6), 150858.
5. Lippi, G.; Mattiuzzi, C.; Cervellin, G., Meat consumption and cancer risk: a critical review of published meta-analyses. *Critical Reviews in Oncology/Hematology* **2016,** 97, 1-14.
6. Koual, M.; Tomkiewicz, C.; Cano-Sancho, G.; Antignac, J.-P.; Bats, A.-S.; Coumoul, X., Environmental chemicals, breast cancer progression and drug resistance. *Environmental Health* **2020,** 19, (1), 117.
7. Lewandowska, A. M.; Rudzki, M.; Rudzki, S.; Lewandowski, T.; Laskowska, B., Environmental risk factors for cancer – review paper. *Ann Agric Environ Med.* **2019,** 26, (1), 1-7.
8. Leon, M. E.; Peruga, A.; McNeill, A.; Kralikova, E.; Guha, N.; Minozzi, S.; Espina, C.; Schüz, J., European Code against Cancer, 4th Edition: Tobacco and cancer. *Cancer Epidemiology* **2015,** 39, S20-S33.
9. Masrour-Roudsari, J.; Ebrahimpour, S., Causal role of infectious agents in cancer: An overview. *Caspian journal of internal medicine* **2017,** 8, (3), 153-158.
10. Krakhmal, N. V.; Zavyalova, M. V.; Denisov, E. V.; Vtorushin, S. V.; Perelmuter, V. M., Cancer Invasion: Patterns and Mechanisms. *Acta naturae* **2015,** 7, (2), 17-28.
11. Hanahan, D., Hallmarks of Cancer: New Dimensions. *Cancer Discovery* **2022,** 12, (1), 31-46.
12. Sarkar, S.; Horn, G.; Moulton, K.; Oza, A.; Byler, S.; Kokolus, S.; Longacre, M., Cancer development, progression, and therapy: an epigenetic overview. *Int J Mol Sci* **2013,** 14, (10), 21087-113.
13. Hanahan, D.; Weinberg, R. A., The Hallmarks of Cancer. *Cell* **2000,** 100, (1), 57-70.

14. Wu, T.; Dai, Y., Tumor microenvironment and therapeutic response. *Cancer Letters* **2017,** 387, 61-68.
15. Hanahan, D.; Weinberg, Robert A., Hallmarks of Cancer: The Next Generation. *Cell* **2011,** 144, (5), 646-674.
16. DeSantis, C. E.; Lin, C. C.; Mariotto, A. B.; Siegel, R. L.; Stein, K. D.; Kramer, J. L.; Alteri, R.; Robbins, A. S.; Jemal, A., Cancer treatment and survivorship statistics, 2014. *CA: A Cancer Journal for Clinicians* **2014,** 64, (4), 252-271.
17. Neha, D.; Momin, M.; Khan, T.; Gharat, S.; Ningthoujam, R. S.; Omri, A., Metallic nanoparticles as drug delivery system for the treatment of cancer. *Expert Opinion on Drug Delivery* **2021,** 18, (9), 1261-1290.
18. Lin, Q.; Jia, M.; Fu, Y.; Li, B.; Dong, Z.; Niu, X.; You, Z., Upper-Critical-Solution-Temperature Polymer Modified Gold Nanorods for Laser Controlled Drug Release and Enhanced Anti-Tumour Therapy. *Frontiers in Pharmacology* **2021,** 12.
19. Xu, J.-J.; Zhang, W.-C.; Guo, Y.-W.; Chen, X.-Y.; Zhang, Y.-N., Metal nanoparticles as a promising technology in targeted cancer treatment. *Drug Delivery* **2022,** 29, (1), 664-678.
20. Wang, Y.; Han, Y.; Jin, Y.; He, Q.; Wang, Z., The Advances in Epigenetics for Cancer Radiotherapy. *International Journal of Molecular Sciences* **2022,** 23, (10), 5654.
21. Li, Z.; Tan, S.; Li, S.; Shen, Q.; Wang, K., Cancer drug delivery in the nano era: An overview and perspectives (Review). *Oncol Rep* **2017,** 38, (2), 611-624.
22. Sun, L.; Wang, D.; Chen, Y.; Wang, L.; Huang, P.; Li, Y.; Liu, Z.; Yao, H.; Shi, J., Core-shell hierarchical mesostructured silica nanoparticles for gene/chemo-synergetic stepwise therapy of multidrug-resistant cancer. *Biomaterials* **2017,** 133, 219-228.
23. Bukowski, K.; Kciuk, M.; Kontek, R., Mechanisms of Multidrug Resistance in Cancer Chemotherapy. *International Journal of Molecular Sciences* **2020,** 21, (9), 3233.
24. Aghebati-Maleki, A.; Dolati, S.; Ahmadi, M.; Baghbanzhadeh, A.; Asadi, M.; Fotouhi, A.; Yousefi, M.; Aghebati-Maleki, L., Nanoparticles and cancer therapy: Perspectives for application of nanoparticles in the treatment of cancers. *J Cell Physiol* **2020,** 235, (3), 1962-1972.
25. Goncalves, A. S. C.; Rodrigues, C. F.; Moreira, A. F.; Correia, I. J., Strategies to improve the photothermal capacity of gold-based nanomedicines. *Acta Biomater* **2020,** 116, 105-137.

26. Guimaraes, R. S.; Rodrigues, C. F.; Moreira, A. F.; Correia, I. J., Overview of stimuli-responsive mesoporous organosilica nanocarriers for drug delivery. *Pharmacol Res* **2020,** 155, 104742.
27. Huang, N.; Liu, Y.; Fang, Y.; Zheng, S.; Wu, J.; Wang, M.; Zhong, W.; Shi, M.; Xing, M.; Liao, W., Gold Nanoparticles Induce Tumor Vessel Normalization and Impair Metastasis by Inhibiting Endothelial Smad2/3 Signaling. *ACS Nano* **2020,** 14, (7), 7940-7958.
28. Rodrigues, C. F.; Alves, C. G.; Lima-Sousa, R.; Moreira, A. F.; de Melo-Diogo, D.; Correia, I. J., Chapter 10 - Inorganic-based drug delivery systems for cancer therapy. In *Advances and Avenues in the Development of Novel Carriers for Bioactives and Biological Agents*, Singh, M. R.; Singh, D.; Kanwar, J. R.; Chauhan, N. S., Eds. Academic Press: 2020; pp 283-316.
29. Fernandes, N.; Rodrigues, C. F.; de Melo-Diogo, D.; Correia, I. J.; Moreira, A. F., Optimization of the GSH-Mediated Formation of Mesoporous Silica-Coated Gold Nanoclusters for NIR Light-Triggered Photothermal Applications. *Nanomaterials* **2021,** 11, (8), 1946.
30. Subhan, M. A.; Yalamarty, S. S. K.; Filipczak, N.; Parveen, F.; Torchilin, V. P., Recent Advances in Tumor Targeting via EPR Effect for Cancer Treatment. *Journal of Personalized Medicine* **2021,** 11, (6), 571.
31. Soares, S.; Sousa, J.; Pais, A.; Vitorino, C., Nanomedicine: Principles, Properties, and Regulatory Issues. *Frontiers in Chemistry* **2018,** 6.
32. Wu, J., The Enhanced Permeability and Retention (EPR) Effect: The Significance of the Concept and Methods to Enhance Its Application. *Journal of Personalized Medicine* **2021,** 11, (8), 771.
33. He, C.; Hu, Y.; Yin, L.; Tang, C.; Yin, C., Effects of particle size and surface charge on cellular uptake and biodistribution of polymeric nanoparticles. *Biomaterials* **2010,** 31, (13), 3657-3666.
34. Xiao, K.; Li, Y.; Luo, J.; Lee, J. S.; Xiao, W.; Gonik, A. M.; Agarwal, R. G.; Lam, K. S., The effect of surface charge on in vivo biodistribution of PEG-oligocholic acid based micellar nanoparticles. *Biomaterials* **2011,** 32, (13), 3435-3446.
35. Spielman-Sun, E.; Avellan, A.; Bland, G. D.; Tappero, R. V.; Acerbo, A. S.; Unrine, J. M.; Giraldo, J. P.; Lowry, G. V., Nanoparticle surface charge influences translocation and leaf distribution in vascular plants with contrasting anatomy. *Environmental Science: Nano* **2019,** 6, (8), 2508-2519.
36. Duan, X.; Li, Y., Physicochemical Characteristics of Nanoparticles Affect Circulation, Biodistribution, Cellular Internalization, and Trafficking. *Small* **2013,** 9, (9-10), 1521-1532.

37. Ma, N.; Ma, C.; Li, C.; Wang, T.; Tang, Y.; Wang, H.; Moul, X.; Chen, Z.; Hel, N., Influence of nanoparticle shape, size, and surface functionalization on cellular uptake. *J Nanosci Nanotechnol* **2013,** 13, (10), 6485-98.
38. Black, K. C. L.; Wang, Y.; Luehmann, H. P.; Cai, X.; Xing, W.; Pang, B.; Zhao, Y.; Cutler, C. S.; Wang, L. V.; Liu, Y.; Xia, Y., Radioactive 198Au-Doped Nanostructures with Different Shapes for In Vivo Analyses of Their Biodistribution, Tumor Uptake, and Intratumoral Distribution. *ACS Nano* **2014,** 8, (5), 4385-4394.
39. Li, Y.; Kröger, M.; Liu, W. K., Shape effect in cellular uptake of PEGylated nanoparticles: comparison between sphere, rod, cube and disk. *Nanoscale* **2015,** 7, (40), 16631-16646.
40. Barbero, F.; Russo, L.; Vitali, M.; Piella, J.; Salvo, I.; Borrajo, M. L.; Busquets-Fité, M.; Grandori, R.; Bastús, N. G.; Casals, E.; Puntes, V., Formation of the Protein Corona: The Interface between Nanoparticles and the Immune System. *Seminars in Immunology* **2017,** 34, 52-60.
41. Farshbaf, M.; Valizadeh, H.; Panahi, Y.; Fatahi, Y.; Chen, M.; Zarebkohan, A.; Gao, H., The impact of protein corona on the biological behavior of targeting nanomedicines. *International Journal of Pharmaceutics* **2022,** 614, 121458.
42. Xiao, Q.; Zoulikha, M.; Qiu, M.; Teng, C.; Lin, C.; Li, X.; Sallam, M. A.; Xu, Q.; He, W., The effects of protein corona on in vivo fate of nanocarriers. *Advanced Drug Delivery Reviews* **2022,** 186, 114356.
43. Mout, R.; Moyano, D. F.; Rana, S.; Rotello, V. M., Surface functionalization of nanoparticles for nanomedicine. *Chemical Society Reviews* **2012,** 41, (7), 2539-2544.
44. Li, S.; Zhang, L., Erythrocyte membrane nano-capsules: biomimetic delivery and controlled release of photothermal–photochemical coupling agents for cancer cell therapy. *Dalton Transactions* **2020,** 49, (8), 2645-2651.
45. Lian, Y.; Wang, X.; Guo, P.; Li, Y.; Raza, F.; Su, J.; Qiu, M., Erythrocyte Membrane-Coated Arsenic Trioxide-Loaded Sodium Alginate Nanoparticles for Tumor Therapy. *Pharmaceutics* **2020,** 12, (1), 21.
46. Xiao, Y.; Du, J., Superparamagnetic nanoparticles for biomedical applications. *Journal of Materials Chemistry B* **2020,** 8, (3), 354-367.
47. Alexis, F.; Pridgen, E.; Molnar, L. K.; Farokhzad, O. C., Factors Affecting the Clearance and Biodistribution of Polymeric Nanoparticles. *Molecular Pharmaceutics* **2008,** 5, (4), 505-515.

48. Goddard, Z. R.; Marín, M. J.; Russell, D. A.; Searcey, M., Active targeting of gold nanoparticles as cancer therapeutics. *Chemical Society Reviews* **2020,** 49, (23), 8774-8789.
49. Mahon, E.; Salvati, A.; Baldelli Bombelli, F.; Lynch, I.; Dawson, K. A., Designing the nanoparticle–biomolecule interface for "targeting and therapeutic delivery". *Journal of Controlled Release* **2012,** 161, (2), 164-174.
50. Steichen, S. D.; Caldorera-Moore, M.; Peppas, N. A., A review of current nanoparticle and targeting moieties for the delivery of cancer therapeutics. *European Journal of Pharmaceutical Sciences* **2013,** 48, (3), 416-427.
51. Koo, H.; Huh, M. S.; Sun, I.-C.; Yuk, S. H.; Choi, K.; Kim, K.; Kwon, I. C., In Vivo Targeted Delivery of Nanoparticles for Theranosis. *Accounts of Chemical Research* **2011,** 44, (10), 1018-1028.
52. Liu, X.; Yan, B.; Li, Y.; Ma, X.; Jiao, W.; Shi, K.; Zhang, T.; Chen, S.; He, Y.; Liang, X. J.; Fan, H., Graphene Oxide-Grafted Magnetic Nanorings Mediated Magnetothermodynamic Therapy Favoring Reactive Oxygen Species-Related Immune Response for Enhanced Antitumor Efficacy. *ACS Nano* **2020,** 14, (2), 1936-1950.
53. Li, G.; Zhong, X.; Wang, X.; Gong, F.; Lei, H.; Zhou, Y.; Li, C.; Xiao, Z.; Ren, G.; Zhang, L.; Dong, Z.; Liu, Z.; Cheng, L., Titanium carbide nanosheets with defect structure for photothermal-enhanced sonodynamic therapy. *Bioact Mater* **2022,** 8, 409-419.
54. Loh, X. J.; Lee, T. C.; Dou, Q.; Deen, G. R., Utilising inorganic nanocarriers for gene delivery. *Biomater Sci* **2016,** 4, (1), 70-86.
55. Liou, G. Y.; Storz, P., Reactive oxygen species in cancer. *Free Radic Res* **2010,** 44, (5), 479-96.
56. Tricoli, A.; Righettoni, M.; Teleki, A., Semiconductor gas sensors: dry synthesis and application. *Angew Chem Int Ed Engl* **2010,** 49, (42), 7632-59.
57. Huynh, K. H.; Pham, X. H.; Kim, J.; Lee, S. H.; Chang, H.; Rho, W. Y.; Jun, B. H., Synthesis, Properties, and Biological Applications of Metallic Alloy Nanoparticles. *Int J Mol Sci* **2020,** 21, (14).
58. Amendola, V.; Meneghetti, M., Laser ablation synthesis in solution and size manipulation of noble metal nanoparticles. *Phys Chem Chem Phys* **2009,** 11, (20), 3805-21.
59. Annamalai, J.; Murugan, P.; Ganapathy, D.; Nallaswamy, D.; Atchudan, R.; Arya, S.; Khosla, A.; Barathi, S.; Sundramoorthy, A. K., Synthesis of various dimensional metal organic frameworks (MOFs) and their hybrid composites for emerging applications - A review. *Chemosphere* **2022,** 298, 134184.

60. Hu, P.; Chen, L.; Kang, X.; Chen, S., Surface Functionalization of Metal Nanoparticles by Conjugated Metal-Ligand Interfacial Bonds: Impacts on Intraparticle Charge Transfer. *Acc Chem Res* **2016,** 49, (10), 2251-2260.
61. Neha, D.; Momin, M.; Khan, T.; Gharat, S.; Ningthoujam, R. S.; Omri, A., Metallic nanoparticles as drug delivery system for the treatment of cancer. *Expert Opin Drug Deliv* **2021,** 18, (9), 1261-1290.
62. Xu, J. J.; Zhang, W. C.; Guo, Y. W.; Chen, X. Y.; Zhang, Y. N., Metal nanoparticles as a promising technology in targeted cancer treatment. *Drug Deliv* **2022,** 29, (1), 664-678.
63. Anselmo, A. C.; Mitragotri, S., A Review of Clinical Translation of Inorganic Nanoparticles. *AAPS J* **2015,** 17, (5), 1041-54.
64. Canaparo, R.; Foglietta, F.; Limongi, T.; Serpe, L., Biomedical Applications of Reactive Oxygen Species Generation by Metal Nanoparticles. *Materials (Basel)* **2020,** 14, (1).
65. Gonzalez-Rubio, G.; Guerrero-Martinez, A.; Liz-Marzan, L. M., Reshaping, Fragmentation, and Assembly of Gold Nanoparticles Assisted by Pulse Lasers. *Acc Chem Res* **2016,** 49, (4), 678-86.
66. Bhatia, S., Natural Polymers vs Synthetic Polymer. **2016**, 95-118.
67. Aslan, N.; Ceylan, B.; Koç, M. M.; Findik, F., Metallic nanoparticles as X-Ray computed tomography (CT) contrast agents: A review. *Journal of Molecular Structure* **2020,** 1219, 128599.
68. Liu, Y.; Ai, K.; Lu, L., Nanoparticulate X-ray computed tomography contrast agents: from design validation to in vivo applications. *Acc Chem Res* **2012,** 45, (10), 1817-27.
69. Cheheltani, R.; Ezzibdeh, R. M.; Chhour, P.; Pulaparthi, K.; Kim, J.; Jurcova, M.; Hsu, J. C.; Blundell, C.; Litt, H. I.; Ferrari, V. A.; Allcock, H. R.; Sehgal, C. M.; Cormode, D. P., Tunable, biodegradable gold nanoparticles as contrast agents for computed tomography and photoacoustic imaging. *Biomaterials* **2016,** 102, 87-97.
70. De La Vega, J. C.; Esquinas, P. L.; Gill, J. K.; Jessa, S.; Gill, B.; Thakur, Y.; Saatchi, K.; Hafeli, U. O., Comparison of Rhenium and Iodine as Contrast Agents in X-Ray Imaging. *Contrast Media Mol Imaging* **2021,** 2021, 1250360.
71. Berger, M.; Bauser, M.; Frenzel, T.; Hilger, C. S.; Jost, G.; Lauria, S.; Morgenstern, B.; Neis, C.; Pietsch, H.; Sulzle, D.; Hegetschweiler, K., Hafnium-Based Contrast Agents for X-ray Computed Tomography. *Inorg Chem* **2017,** 56, (10), 5757-5761.

72. Bae, K. T.; McDermott, R.; Gierada, D. S.; Heiken, J. P.; Nolte, M. A.; Takahashi, N.; Hong, C., Gadolinium-enhanced computed tomography angiography in multi-detector row computed tomography. *Academic Radiology* **2004,** 11, (1), 61-68.
73. Werts, M. H. V.; Allix, F.; Francais, O.; Frochot, C.; Griscom, L.; Le Pioufle, B.; Loumaigne, M.; Midelet, J., Manipulation and Optical Detection of Colloidal Functional Plasmonic Nanostructures in Microfluidic Systems. *IEEE Journal of Selected Topics in Quantum Electronics* **2014,** 20, (3), 102-114.
74. Wang, L.; Hasanzadeh Kafshgari, M.; Meunier, M., Optical Properties and Applications of Plasmonic-Metal Nanoparticles. *Advanced Functional Materials* **2020,** 30, (51), 2005400.
75. Noguez, C., Surface Plasmons on Metal Nanoparticles: The Influence of Shape and Physical Environment. *The Journal of Physical Chemistry C* **2007,** 111, (10), 3806-3819.
76. Liz-Marzán, L. M., Tailoring Surface Plasmons through the Morphology and Assembly of Metal Nanoparticles. *Langmuir* **2006,** 22, (1), 32-41.
77. Liang, J.; Liu, H.; Yu, J.; Zhou, L.; Zhu, J., Plasmon-enhanced solar vapor generation. *Nanophotonics* **2019,** 8, (5), 771-786.
78. Jeong, Y.; Kook, Y. M.; Lee, K.; Koh, W. G., Metal enhanced fluorescence (MEF) for biosensors: General approaches and a review of recent developments. *Biosens Bioelectron* **2018,** 111, 102-116.
79. Lin, Q.; Jia, M.; Fu, Y.; Li, B.; Dong, Z.; Niu, X.; You, Z., Upper-Critical-Solution-Temperature Polymer Modified Gold Nanorods for Laser Controlled Drug Release and Enhanced Anti-Tumour Therapy. *Front Pharmacol* **2021,** 12, 738630.
80. de Melo-Diogo, D.; Pais-Silva, C.; Dias, D. R.; Moreira, A. F.; Correia, I. J., Strategies to Improve Cancer Photothermal Therapy Mediated by Nanomaterials. *Advanced Healthcare Materials* **2017,** 6, (10), 1700073.
81. Bettaieb, A.; K, P.; A, D., Hyperthermia: Cancer Treatment and Beyond. **2013**.
82. Zhang, Y.; Zhan, X.; Xiong, J.; Peng, S.; Huang, W.; Joshi, R.; Cai, Y.; Liu, Y.; Li, R.; Yuan, K.; Zhou, N.; Min, W., Temperature-dependent cell death patterns induced by functionalized gold nanoparticle photothermal therapy in melanoma cells. *Sci Rep* **2018,** 8, (1), 8720.
83. Fernandes, N.; Rodrigues, C. F.; Moreira, A. F.; Correia, I. J., Overview of the application of inorganic nanomaterials in cancer photothermal therapy. *Biomater Sci* **2020,** 8, (11), 2990-3020.

84. Xing, Y.; Cai, Z.; Xu, M.; Ju, W.; Luo, X.; Hu, Y.; Liu, X.; Kang, T.; Wu, P.; Cai, C.; Zhu, J. J., Raman observation of a molecular signaling pathway of apoptotic cells induced by photothermal therapy. *Chem Sci* **2019,** 10, (47), 10900-10910.
85. Jiang, Z.; Li, T.; Cheng, H.; Zhang, F.; Yang, X.; Wang, S.; Zhou, J.; Ding, Y., Nanomedicine potentiates mild photothermal therapy for tumor ablation. *Asian J Pharm Sci* **2021,** 16, (6), 738-761.
86. Rudakov, G. A.; Tsiberkin, K. B.; Ponomarev, R. S.; Henner, V. K.; Ziolkowska, D. A.; Jasinski, J. B.; Sumanasekera, G., Magnetic properties of transition metal nanoparticles enclosed in carbon nanocages. *Journal of Magnetism and Magnetic Materials* **2019,** 472, 34-39.
87. Soheilian, R.; Choi, Y. S.; David, A. E.; Abdi, H.; Maloney, C. E.; Erb, R. M., Toward Accumulation of Magnetic Nanoparticles into Tissues of Small Porosity. *Langmuir* **2015,** 31, (30), 8267-8274.
88. Guo, X.; Li, W.; Luo, L.; Wang, Z.; Li, Q.; Kong, F.; Zhang, H.; Yang, J.; Zhu, C.; Du, Y.; You, J., External Magnetic Field-Enhanced Chemo-Photothermal Combination Tumor Therapy via Iron Oxide Nanoparticles. *ACS Applied Materials & Interfaces* **2017,** 9, (19), 16581-16593.
89. Farzin, A.; Etesami, S. A.; Quint, J.; Memic, A.; Tamayol, A., Magnetic Nanoparticles in Cancer Therapy and Diagnosis. *Adv Healthc Mater* **2020,** 9, (9), e1901058.
90. Sengul, A. B.; Asmatulu, E., Toxicity of metal and metal oxide nanoparticles: a review. *Environmental Chemistry Letters* **2020,** 18, (5), 1659-1683.
91. Wu, H.; Yin, J. J.; Wamer, W. G.; Zeng, M.; Lo, Y. M., Reactive oxygen species-related activities of nano-iron metal and nano-iron oxides. *J Food Drug Anal* **2014,** 22, (1), 86-94.
92. Yuan, P.; Ding, X.; Yang, Y. Y.; Xu, Q.-H., Metal Nanoparticles for Diagnosis and Therapy of Bacterial Infection. *Advanced Healthcare Materials* **2018,** 7, (13), 1701392.
93. Juarranz, Á.; Jaén, P.; Sanz-Rodríguez, F.; Cuevas, J.; González, S., Photodynamic therapy of cancer. Basic principles and applications. *Clinical and Translational Oncology* **2008,** 10, (3), 148-154.
94. Wilson, B. C., Photodynamic Therapy for Cancer: Principles. *Canadian Journal of Gastroenterology* **2002,** 16, 743109.
95. Vinković Vrček, I.; Pavičić, I.; Crnković, T.; Jurašin, D.; Babič, M.; Horák, D.; Lovrić, M.; Ferhatović, L.; Ćurlin, M.; Gajović, S., Does surface coating of metallic nanoparticles modulate their interference with in vitro assays? *RSC Advances* **2015,** 5, (87), 70787-70807.

96. Rajendran, K.; Pujari, L.; Krishnamoorthy, M.; Sen, S.; Dharmaraj, D.; Karuppiah, K.; Ethiraj, K., Toxicological evaluation of biosynthesised hematite nanoparticles in vivo. *Colloids and Surfaces B: Biointerfaces* **2021,** 198, 111475.
97. García-Álvarez, R.; Hadjidemetriou, M.; Sánchez-Iglesias, A.; Liz-Marzán, L. M.; Kostarelos, K., In vivo formation of protein corona on gold nanoparticles. The effect of their size and shape. *Nanoscale* **2018,** 10, (3), 1256-1264.
98. Thambiraj, S.; Vijayalakshmi, R.; Ravi Shankaran, D., An effective strategy for development of docetaxel encapsulated gold nanoformulations for treatment of prostate cancer. *Sci Rep* **2021,** 11, (1), 2808.
99. Hada, A. M.; Craciun, A. M.; Focsan, M.; Borlan, R.; Soritau, O.; Todea, M.; Astilean, S., Folic acid functionalized gold nanoclusters for enabling targeted fluorescence imaging of human ovarian cancer cells. *Talanta* **2021,** 225, 121960.
100. Kim, H. S.; Lee, S. J.; Lee, D. Y., Milk protein-shelled gold nanoparticles with gastrointestinally active absorption for aurotherapy to brain tumor. *Bioact Mater* **2022,** 8, 35-48.
101. Mapanao, A. K.; Santi, M.; Voliani, V., Combined chemo-photothermal treatment of three-dimensional head and neck squamous cell carcinomas by gold nano-architectures. *J Colloid Interface Sci* **2021,** 582, (Pt B), 1003-1011.
102. You, Y. H.; Lin, Y. F.; Nirosha, B.; Chang, H. T.; Huang, Y. F., Polydopamine-coated gold nanostar for combined antitumor and antiangiogenic therapy in multidrug-resistant breast cancer. *Nanotheranostics* **2019,** 3, (3), 266-283.
103. Sheng, Y.; Liu, C.; Yuan, Y.; Tao, X.; Yang, F.; Shan, X.; Zhou, H.; Xu, F., Long-circulating polymeric nanoparticles bearing a combinatorial coating of PEG and water-soluble chitosan. *Biomaterials* **2009,** 30, (12), 2340-8.
104. Li, B.; Xie, J.; Yuan, Z.; Jain, P.; Lin, X.; Wu, K.; Jiang, S., Mitigation of Inflammatory Immune Responses with Hydrophilic Nanoparticles. *Angewandte Chemie International Edition* **2018,** 57, (17), 4527-4531.
105. Lowe, S.; O'Brien-Simpson, N. M.; Connal, L. A., Antibiofouling polymer interfaces: poly(ethylene glycol) and other promising candidates. *Polymer Chemistry* **2015,** 6, (2), 198-212.
106. Yu, Y.; Luan, Y.; Dai, W., Dynamic process, mechanisms, influencing factors and study methods of protein corona formation. *Int J Biol Macromol* **2022,** 205, 731-739.
107. Feng, W.; Zhu, S.; Ishihara, K.; Brash, J. L., Protein resistant surfaces: comparison of acrylate graft polymers bearing oligo-ethylene oxide and phosphorylcholine side chains. *Biointerphases* **2006,** 1, (1), 50.

108. He, M.; Gao, K.; Zhou, L.; Jiao, Z.; Wu, M.; Cao, J.; You, X.; Cai, Z.; Su, Y.; Jiang, Z., Zwitterionic materials for antifouling membrane surface construction. *Acta Biomater* **2016,** 40, 142-152.
109. Zhang, Y.; Liu, Y.; Ren, B.; Zhang, D.; Xie, S.; Chang, Y.; Yang, J.; Wu, J.; Xu, L.; Zheng, J., Fundamentals and applications of zwitterionic antifouling polymers. *Journal of Physics D: Applied Physics* **2019,** 52, (40), 403001.
110. Liu, X.; Li, H.; Chen, Y.; Jin, Q.; Ren, K.; Ji, J., Mixed-Charge Nanoparticles for Long Circulation, Low Reticuloendothelial System Clearance, and High Tumor Accumulation. *Advanced Healthcare Materials* **2014,** 3, (9), 1439-1447.
111. Wu, L.; Lin, B.; Yang, H.; Chen, J.; Mao, Z.; Wang, W.; Gao, C., Enzyme-responsive multifunctional peptide coating of gold nanorods improves tumor targeting and photothermal therapy efficacy. *Acta Biomater* **2019,** 86, 363-372.
112. Li, W.; Cao, Z.; Yu, L.; Huang, Q.; Zhu, D.; Lu, C.; Lu, A.; Liu, Y., Hierarchical drug release designed Au @PDA-PEG-MTX NPs for targeted delivery to breast cancer with combined photothermal-chemotherapy. *J Nanobiotechnology* **2021,** 19, (1), 143.
113. Sathiyaseelan, A.; Saravanakumar, K.; Mariadoss, A. V. A.; Wang, M. H., pH-controlled nucleolin targeted release of dual drug from chitosan-gold based aptamer functionalized nano drug delivery system for improved glioblastoma treatment. *Carbohydr Polym* **2021,** 262, 117907.
114. Feng, Y.; Cheng, Y.; Chang, Y.; Jian, H.; Zheng, R.; Wu, X.; Xu, K.; Wang, L.; Ma, X.; Li, X.; Zhang, H., Time-staggered delivery of erlotinib and doxorubicin by gold nanocages with two smart polymers for reprogrammable release and synergistic with photothermal therapy. *Biomaterials* **2019,** 217, 119327.
115. Wang, N.; Shi, J.; Wu, C.; Chu, W.; Tao, W.; Li, W.; Yuan, X., Design of DOX-GNRs-PNIPAM@PEG-PLA Micelle With Temperature and Light Dual-Function for Potent Melanoma Therapy. *Front Chem* **2020,** 8, 599740.
116. Li, D.; Zhang, R.; Liu, G.; Kang, Y.; Wu, J., Redox-Responsive Self-Assembled Nanoparticles for Cancer Therapy. *Advanced Healthcare Materials* **2020,** 9, (20), 2000605.
117. Shi, Y.; van der Meel, R.; Chen, X.; Lammers, T., The EPR effect and beyond: Strategies to improve tumor targeting and cancer nanomedicine treatment efficacy. *Theranostics* **2020,** 10, (17), 7921-7924.
118. Acharya, S.; Sahoo, S. K., PLGA nanoparticles containing various anticancer agents and tumour delivery by EPR effect. *Adv Drug Deliv Rev* **2011,** 63, (3), 170-83.

119. Yucel, O.; Sengelen, A.; Emik, S.; Onay-Ucar, E.; Arda, N.; Gurdag, G., Folic acid-modified methotrexate-conjugated gold nanoparticles as nano-sized trojans for drug delivery to folate receptor-positive cancer cells. *Nanotechnology* **2020,** 31, (35), 355101.
120. Mulens-Arias, V.; Nicolas-Boluda, A.; Pinto, A.; Balfourier, A.; Carn, F.; Silva, A. K. A.; Pocard, M.; Gazeau, F., Tumor-Selective Immune-Active Mild Hyperthermia Associated with Chemotherapy in Colon Peritoneal Metastasis by Photoactivation of Fluorouracil-Gold Nanoparticle Complexes. *ACS Nano* **2021,** 15, (2), 3330-3348.
121. Guo, J.; Rahme, K.; He, Y.; Li, L. L.; Holmes, J. D.; O'Driscoll, C. M., Gold nanoparticles enlighten the future of cancer theranostics. *Int J Nanomedicine* **2017,** 12, 6131-6152.
122. Cole, L. E.; Ross, R. D.; Tilley, J. M. R.; Vargo-Gogola, T.; Roeder, R. K., Gold nanoparticles as contrast agents in x-ray imaging and computed tomography. *Nanomedicine* **2015,** 10, (2), 321-341.
123. Xi, D.; Dong, S.; Meng, X.; Lu, Q.; Meng, L.; Ye, J., Gold nanoparticles as computerized tomography (CT) contrast agents. *RSC Advances* **2012,** 2, (33), 12515.
124. Capek, I., Polymer decorated gold nanoparticles in nanomedicine conjugates. *Adv Colloid Interface Sci* **2017,** 249, 386-399.
125. Guo, C.; Hall, G. N.; Addison, J. B.; Yarger, J. L., Gold nanoparticle-doped silk film as biocompatible SERS substrate. *RSC Advances* **2015,** 5, (3), 1937-1942.
126. Fernandes, N.; Rodrigues, C. F.; de Melo-Diogo, D.; Correia, I. J.; Moreira, A. F., Optimization of the GSH-Mediated Formation of Mesoporous Silica-Coated Gold Nanoclusters for NIR Light-Triggered Photothermal Applications. *Nanomaterials (Basel)* **2021,** 11, (8).
127. Fernandes, J.; Kang, S., Numerical Study on the Surface Plasmon Resonance Tunability of Spherical and Non-Spherical Core-Shell Dimer Nanostructures. *Nanomaterials* **2021,** 11, (7).
128. Xu, H.; Käll, M., Modeling the optical response of nanoparticle-based surface plasmon resonance sensors. *Sensors and Actuators B: Chemical* **2002,** 87, (2), 244-249.
129. Bouhelier, A.; Bachelot, R.; Lerondel, G.; Kostcheev, S.; Royer, P.; Wiederrecht, G. P., Surface plasmon characteristics of tunable photoluminescence in single gold nanorods. *Phys Rev Lett* **2005,** 95, (26), 267405.

130. Chandrasekaran, R.; Lee, A. S. W.; Yap, L. W.; Jans, D. A.; Wagstaff, K. M.; Cheng, W., Tumor cell-specific photothermal killing by SELEX-derived DNA aptamer-targeted gold nanorods. *Nanoscale* **2016,** 8, (1), 187-196.
131. Shi, W.; Casas, J.; Venkataramasubramani, M.; Tang, L., Synthesis and Characterization of Gold Nanoparticles with Plasmon Absorbance Wavelength Tunable from Visible to Near Infrared Region. *ISRN Nanomaterials* **2012,** 2012, 659043.
132. Jacinto, T. A.; Rodrigues, C. F.; Moreira, A. F.; Miguel, S. P.; Costa, E. C.; Ferreira, P.; Correia, I. J., Hyaluronic acid and vitamin E polyethylene glycol succinate functionalized gold-core silica shell nanorods for cancer targeted photothermal therapy. *Colloids Surf B Biointerfaces* **2020,** 188, 110778.
133. Peng, C.; Zheng, L.; Chen, Q.; Shen, M.; Guo, R.; Wang, H.; Cao, X.; Zhang, G.; Shi, X., PEGylated dendrimer-entrapped gold nanoparticles for in vivo blood pool and tumor imaging by computed tomography. *Biomaterials* **2012,** 33, (4), 1107-19.
134. Gu, W.; Zhang, Q.; Zhang, T.; Li, Y.; Xiang, J.; Peng, R.; Liu, J., Hybrid polymeric nano-capsules loaded with gold nanoclusters and indocyanine green for dual-modal imaging and photothermal therapy. *J Mater Chem B* **2016,** 4, (5), 910-919.
135. Alkhayal, A.; Fathima, A.; Alhasan, A. H.; Alsharaeh, E. H., PEG Coated Fe3O4/RGO Nano-Cube-Like Structures for Cancer Therapy via Magnetic Hyperthermia. *Nanomaterials (Basel)* **2021,** 11, (9).
136. Ebrahiminezhad, A.; Zare-Hoseinabadi, A.; Sarmah, A. K.; Taghizadeh, S.; Ghasemi, Y.; Berenjian, A., Plant-Mediated Synthesis and Applications of Iron Nanoparticles. *Mol Biotechnol* **2018,** 60, (2), 154-168.
137. Zhi, D.; Yang, T.; Yang, J.; Fu, S.; Zhang, S., Targeting strategies for superparamagnetic iron oxide nanoparticles in cancer therapy. *Acta Biomater* **2020,** 102, 13-34.
138. Palanisamy, S.; Wang, Y. M., Superparamagnetic iron oxide nanoparticulate system: synthesis, targeting, drug delivery and therapy in cancer. *Dalton Trans* **2019,** 48, (26), 9490-9515.
139. Habra, K.; McArdle, S. E. B.; Morris, R. H.; Cave, G. W. V., Synthesis and Functionalisation of Superparamagnetic Nano-Rods towards the Treatment of Glioblastoma Brain Tumours. *Nanomaterials (Basel)* **2021,** 11, (9).
140. Vangijzegem, T.; Stanicki, D.; Laurent, S., Magnetic iron oxide nanoparticles for drug delivery: applications and characteristics. *Expert Opin Drug Deliv* **2019,** 16, (1), 69-78.

141. Liu, J. F.; Jang, B.; Issadore, D.; Tsourkas, A., Use of magnetic fields and nanoparticles to trigger drug release and improve tumor targeting. *WIREs Nanomedicine and Nanobiotechnology* **2019,** 11, (6), e1571.
142. Shah, R. R.; Davis, T. P.; Glover, A. L.; Nikles, D. E.; Brazel, C. S., Impact of magnetic field parameters and iron oxide nanoparticle properties on heat generation for use in magnetic hyperthermia. *Journal of Magnetism and Magnetic Materials* **2015,** 387, 96-106.
143. Obaidat, I. M.; Issa, B.; Haik, Y., Magnetic Properties of Magnetic Nanoparticles for Efficient Hyperthermia. *Nanomaterials* **2015,** 5, (1), 63-89.
144. Boyer, C.; Whittaker, M. R.; Bulmus, V.; Liu, J.; Davis, T. P., The design and utility of polymer-stabilized iron-oxide nanoparticles for nanomedicine applications. *NPG Asia Materials* **2010,** 2, (1), 23-30.
145. Xu, X.; Zhou, X.; Xiao, B.; Xu, H.; Hu, D.; Qian, Y.; Hu, H.; Zhou, Z.; Liu, X.; Gao, J.; Slater, N. K. H.; Shen, Y.; Tang, J., Glutathione-Responsive Magnetic Nanoparticles for Highly Sensitive Diagnosis of Liver Metastases. *Nano Lett* **2021,** 21, (5), 2199-2206.
146. Xiao, Z.; You, Y.; Liu, Y.; He, L.; Zhang, D.; Cheng, Q.; Wang, D.; Chen, T.; Shi, C.; Luo, L., NIR-Triggered Blasting Nanovesicles for Targeted Multimodal Image-Guided Synergistic Cancer Photothermal and Chemotherapy. *ACS Appl Mater Interfaces* **2021,** 13, (30), 35376-35388.
147. Chen, L.; Wu, Y.; Wu, H.; Li, J.; Xie, J.; Zang, F.; Ma, M.; Gu, N.; Zhang, Y., Magnetic targeting combined with active targeting of dual-ligand iron oxide nanoprobes to promote the penetration depth in tumors for effective magnetic resonance imaging and hyperthermia. *Acta Biomater* **2019,** 96, 491-504.
148. Yun, B.; Zhu, H.; Yuan, J.; Sun, Q.; Li, Z., Synthesis, modification and bioapplications of nanoscale copper chalcogenides. *J Mater Chem B* **2020,** 8, (22), 4778-4812.
149. Zhou, M.; Tian, M.; Li, C., Copper-Based Nanomaterials for Cancer Imaging and Therapy. *Bioconjugate Chemistry* **2016,** 27, (5), 1188-1199.
150. Rubilar, O.; Rai, M.; Tortella, G.; Diez, M. C.; Seabra, A. B.; Durán, N., Biogenic nanoparticles: copper, copper oxides, copper sulphides, complex copper nanostructures and their applications. *Biotechnol Lett* **2013,** 35, (9), 1365-1375.
151. Tian, H.; Zhang, M.; Jin, G.; Jiang, Y.; Luan, Y., Cu-MOF chemodynamic nanoplatform via modulating glutathione and H2O2 in tumor microenvironment for amplified cancer therapy. *Journal of Colloid and Interface Science* **2021,** 587, 358-366.

152. Wang, S.; Riedinger, A.; Li, H.; Fu, C.; Liu, H.; Li, L.; Liu, T.; Tan, L.; Barthel, M. J.; Pugliese, G.; De Donato, F.; Scotto D'Abbusco, M.; Meng, X.; Manna, L.; Meng, H.; Pellegrino, T., Plasmonic Copper Sulfide Nanocrystals Exhibiting Near-Infrared Photothermal and Photodynamic Therapeutic Effects. *ACS Nano* **2015,** 9, (2), 1788-1800.

153. Egorova, K. S.; Ananikov, V. P., Which Metals are Green for Catalysis? Comparison of the Toxicities of Ni, Cu, Fe, Pd, Pt, Rh, and Au Salts. *Angewandte Chemie International Edition* **2016,** 55, (40), 12150-12162.

154. Letelier, M. E.; Sánchez-Jofré, S.; Peredo-Silva, L.; Cortés-Troncoso, J.; Aracena-Parks, P., Mechanisms underlying iron and copper ions toxicity in biological systems: Pro-oxidant activity and protein-binding effects. *Chemico-Biological Interactions* **2010,** 188, (1), 220-227.

155. Li, W.; Zamani, R.; Rivera Gil, P.; Pelaz, B.; Ibáñez, M.; Cadavid, D.; Shavel, A.; Alvarez-Puebla, R. A.; Parak, W. J.; Arbiol, J.; Cabot, A., CuTe Nanocrystals: Shape and Size Control, Plasmonic Properties, and Use as SERS Probes and Photothermal Agents. *Journal of the American Chemical Society* **2013,** 135, (19), 7098-7101.

156. Li, L.; Rashidi, L. H.; Yao, M.; Ma, L.; Chen, L.; Zhang, J.; Zhang, Y.; Chen, W., CuS nanoagents for photodynamic and photothermal therapies: Phenomena and possible mechanisms. *Photodiagnosis Photodyn Ther* **2017,** 19, 5-14.

157. Shi, H.; Yan, R.; Wu, L.; Sun, Y.; Liu, S.; Zhou, Z.; He, J.; Ye, D., Tumor-targeting CuS nanoparticles for multimodal imaging and guided photothermal therapy of lymph node metastasis. *Acta Biomater* **2018,** 72, 256-265.

158. Yu, X.; Yu, J.; Cheng, B.; Huang, B., One-Pot Template-Free Synthesis of Monodisperse Zinc Sulfide Hollow Spheres and Their Photocatalytic Properties. *Chemistry – A European Journal* **2009,** 15, (27), 6731-6739.

159. Wang, C.-C.; Wang, S.; Xia, Q.; He, W.; Yin, J.-J.; Fu, P. P.; Li, J.-H., Phototoxicity of Zinc Oxide Nanoparticles in HaCaT Keratinocytes-Generation of Oxidative DNA Damage During UVA and Visible Light Irradiation. *Journal of Nanoscience and Nanotechnology* **2013,** 13, (6), 3880-3888.

160. Akhtar, M. J.; Ahamed, M.; Kumar, S.; Khan, M. M.; Ahmad, J.; Alrokayan, S. A., Zinc oxide nanoparticles selectively induce apoptosis in human cancer cells through reactive oxygen species. *Int J Nanomedicine* **2012,** 7, 845-57.

161. Song, T.; Qu, Y.; Ren, Z.; Yu, S.; Sun, M.; Yu, X.; Yu, X., Synthesis and Characterization of Polyvinylpyrrolidone-Modified ZnO Quantum Dots and Their In Vitro Photodynamic Tumor Suppressive Action. *Int J Mol Sci* **2021,** 22, (15).

162. Riddell, I. A.; Lippard, S. J., 1. Cisplatin and Oxaliplatin: Our Current Understanding of Their Actions. **2018**, 1-42.
163. Asharani, P. V.; Xinyi, N.; Hande, M. P.; Valiyaveettil, S., DNA damage and p53-mediated growth arrest in human cells treated with platinum nanoparticles. *Nanomedicine* **2009,** 5, (1), 51-64.
164. Cao, H.; Yang, Y.; Liang, M.; Ma, Y.; Sun, N.; Gao, X.; Li, J., Pt@polydopamine nanoparticles as nanozymes for enhanced photodynamic and photothermal therapy. *Chem Commun (Camb)* **2021,** 57, (2), 255-258.
165. Pedone, D.; Moglianetti, M.; De Luca, E.; Bardi, G.; Pompa, P. P., Platinum nanoparticles in nanobiomedicine. *Chem Soc Rev* **2017,** 46, (16), 4951-4975.
166. Chen, T.; Gu, T.; Cheng, L.; Li, X.; Han, G.; Liu, Z., Porous Pt nanoparticles loaded with doxorubicin to enable synergistic Chemo-/Electrodynamic Therapy. *Biomaterials* **2020,** 255, 120202.
167. Zhu, Y.; Li, W.; Zhao, X.; Zhou, Z.; Wang, Y.; Cheng, Y.; Huang, Q.; Zhang, Q., Hyaluronic Acid-Encapsulated Platinum Nanoparticles for Targeted Photothermal Therapy of Breast Cancer. *J Biomed Nanotechnol* **2017,** 13, (11), 1457-1467.
168. Zhang, X. F.; Liu, Z. G.; Shen, W.; Gurunathan, S., Silver Nanoparticles: Synthesis, Characterization, Properties, Applications, and Therapeutic Approaches. *Int J Mol Sci* **2016,** 17, (9).
169. Kim, S.; Ryu, D.-Y., Silver nanoparticle-induced oxidative stress, genotoxicity and apoptosis in cultured cells and animal tissues. *Journal of Applied Toxicology* **2013,** 33, (2), 78-89.
170. Holmila, R. J.; Vance, S. A.; King, S. B.; Tsang, A. W.; Singh, R.; Furdui, C. M., Silver Nanoparticles Induce Mitochondrial Protein Oxidation in Lung Cells Impacting Cell Cycle and Proliferation. *Antioxidants* **2019,** 8, (11).
171. Park, T.; Lee, S.; Amatya, R.; Cheong, H.; Moon, C.; Kwak, H. D.; Min, K. A.; Shin, M. C., ICG-Loaded PEGylated BSA-Silver Nanoparticles for Effective Photothermal Cancer Therapy. *Int J Nanomedicine* **2020,** 15, 5459-5471.
172. Anselmo, A. C.; Mitragotri, S., Nanoparticles in the clinic: An update post COVID-19 vaccines. *Bioeng Transl Med* **2021,** 6, (3), e10246.
173. Rodallec, A.; Benzekry, S.; Lacarelle, B.; Ciccolini, J.; Fanciullino, R., Pharmacokinetics variability: Why nanoparticles are not just magic-bullets in oncology. *Crit Rev Oncol Hematol* **2018,** 129, 1-12.
174. Wilhelm, S.; Tavares, A. J.; Dai, Q.; Ohta, S.; Audet, J.; Dvorak, H. F.; Chan, W. C. W., Analysis of nanoparticle delivery to tumours. *Nature Reviews Materials* **2016,** 1, (5), 16014.

175. Shi, J.; Kantoff, P. W.; Wooster, R.; Farokhzad, O. C., Cancer nanomedicine: progress, challenges and opportunities. *Nat Rev Cancer* **2017,** 17, (1), 20-37.
176. Rastinehad, A. R.; Anastos, H.; Wajswol, E.; Winoker, J. S.; Sfakianos, J. P.; Doppalapudi, S. K.; Carrick, M. R.; Knauer, C. J.; Taouli, B.; Lewis, S. C.; Tewari, A. K.; Schwartz, J. A.; Canfield, S. E.; George, A. K.; West, J. L.; Halas, N. J., Gold nanoshell-localized photothermal ablation of prostate tumors in a clinical pilot device study. *Proceedings of the National Academy of Sciences* **2019,** 116, (37), 18590-18596.
177. Bayda, S.; Hadla, M.; Palazzolo, S.; Riello, P.; Corona, G.; Toffoli, G.; Rizzolio, F., Inorganic Nanoparticles for Cancer Therapy: A Transition from Lab to Clinic. *Curr Med Chem* **2018,** 25, (34), 4269-4303.
178. Kumthekar, P.; Ko, C. H.; Paunesku, T.; Dixit, K.; Sonabend, A. M.; Bloch, O.; Tate, M.; Schwartz, M.; Zuckerman, L.; Lezon, R.; Lukas, R. V.; Jovanovic, B.; McCortney, K.; Colman, H.; Chen, S.; Lai, B.; Antipova, O.; Deng, J.; Li, L.; Tommasini-Ghelfi, S.; Hurley, L. A.; Unruh, D.; Sharma, N. V.; Kandpal, M.; Kouri, F. M.; Davuluri, R. V.; Brat, D. J.; Muzzio, M.; Glass, M.; Vijayakumar, V.; Heidel, J.; Giles, F. J.; Adams, A. K.; James, C. D.; Woloschak, G. E.; Horbinski, C.; Stegh, A. H., A first-in-human phase 0 clinical study of RNA interference-based spherical nucleic acids in patients with recurrent glioblastoma. *Sci Transl Med* **2021,** 13, (584).
179. Kumthekar, P.; Rademaker, A.; Ko, C.; Dixit, K.; Schwartz, M. A.; Sonabend, A. M.; Sharp, L.; Lukas, R. V.; Stupp, R.; Horbinski, C.; McCortney, K.; Stegh, A. H., A phase 0 first-in-human study using NU-0129: A gold base spherical nucleic acid (SNA) nanoconjugate targeting BCL2L12 in recurrent glioblastoma patients. *Journal of Clinical Oncology* **2019,** 37, (15_suppl), 3012-3012.
180. F Rodrigues, C.; Fernandes, N.; de Melo-Diogo, D.; Ferreira, P.; J Correia, I.; F Moreira, A., HA/PEI-coated acridine orange-loaded gold-core silica shell nanorods for cancer-targeted photothermal and chemotherapy. *Nanomedicine* **2021,** 16, (29), 2569-2586.
181. Pan, Y.; Ma, X.; Liu, C.; Xing, J.; Zhou, S.; Parshad, B.; Schwerdtle, T.; Li, W.; Wu, A.; Haag, R., Retinoic Acid-Loaded Dendritic Polyglycerol-Conjugated Gold Nanostars for Targeted Photothermal Therapy in Breast Cancer Stem Cells. *ACS Nano* **2021,** 15, (9), 15069-15084.
182. Tan, H.; Hou, N.; Liu, Y.; Liu, B.; Cao, W.; Zheng, D.; Li, W.; Liu, Y.; Xu, B.; Wang, Z.; Cui, D., CD133 antibody targeted delivery of gold nanostars loading IR820 and docetaxel for multimodal imaging and near-infrared

photodynamic/photothermal/chemotherapy against castration resistant prostate cancer. *Nanomedicine* **2020,** 27, 102192.

183. Cheng, Y.; Bao, D.; Chen, X.; Wu, Y.; Wei, Y.; Wu, Z.; Li, F.; Piao, J. G., Microwave-triggered/HSP-targeted gold nano-system for triple-negative breast cancer photothermal therapy. *Int J Pharm* **2021,** 593, 120162.
184. Zhang, Y.; Hu, H.; Tang, W.; Zhang, Q.; Li, M.; Jin, H.; Huang, Z.; Cui, Z.; Xu, J.; Wang, K.; Shi, C., A multifunctional magnetic nanosystem based on "two strikes" effect for synergistic anticancer therapy in triple-negative breast cancer. *J Control Release* **2020,** 322, 401-415.
185. Zheng, D.; Wan, C.; Yang, H.; Xu, L.; Dong, Q.; Du, C.; Du, J.; Li, F., Her2-Targeted Multifunctional Nano-Theranostic Platform Mediates Tumor Microenvironment Remodeling and Immune Activation for Breast Cancer Treatment. *Int J Nanomedicine* **2020,** 15, 10007-10028.
186. He, Y.; Wang, M.; Fu, M.; Yuan, X.; Luo, Y.; Qiao, B.; Cao, J.; Wang, Z.; Hao, L.; Yuan, G., Iron(II) phthalocyanine Loaded and AS1411 Aptamer Targeting Nanoparticles: A Nanocomplex for Dual Modal Imaging and Photothermal Therapy of Breast Cancer. *Int J Nanomedicine* **2020,** 15, 5927-5949.
187. Ding, X.; Jiang, W.; Dong, L.; Hong, C.; Luo, Z.; Hu, Y.; Cai, K., Redox-responsive magnetic nanovectors self-assembled from amphiphilic polymer and iron oxide nanoparticles for a remotely targeted delivery of paclitaxel. *J Mater Chem B* **2021,** 9, (30), 6037-6043.
188. Lin, C. H.; Chen, Y. C.; Huang, P. I., Preparation of Multifunctional Dopamine-Coated Zerovalent Iron/Reduced Graphene Oxide for Targeted Phototheragnosis in Breast Cancer. *Nanomaterials (Basel)* **2020,** 10, (10).
189. Xu, J.; Shi, R.; Chen, G.; Dong, S.; Yang, P.; Zhang, Z.; Niu, N.; Gai, S.; He, F.; Fu, Y.; Lin, J., All-in-One Theranostic Nanomedicine with Ultrabright Second Near-Infrared Emission for Tumor-Modulated Bioimaging and Chemodynamic/Photodynamic Therapy. *ACS Nano* **2020,** 14, (8), 9613-9625.
190. Liang, S.; Deng, X.; Chang, Y.; Sun, C.; Shao, S.; Xie, Z.; Xiao, X.; Ma, P.; Zhang, H.; Cheng, Z.; Lin, J., Intelligent Hollow Pt-CuS Janus Architecture for Synergistic Catalysis-Enhanced Sonodynamic and Photothermal Cancer Therapy. *Nano Lett* **2019,** 19, (6), 4134-4145.
191. Poudel, K.; Thapa, R. K.; Gautam, M.; Ou, W.; Soe, Z. C.; Gupta, B.; Ruttala, H. B.; Thuy, H. N.; Dai, P. C.; Jeong, J. H.; Ku, S. K.; Choi, H. G.; Yong, C. S.; Kim, J. O., Multifaceted NIR-responsive polymer-peptide-enveloped drug-loaded copper sulfide nanoplatform for chemo-phototherapy against highly tumorigenic prostate cancer. *Nanomedicine* **2019,** 21, 102042.

192. Maor, I.; Asadi, S.; Korganbayev, S.; Dahis, D.; Shamay, Y.; Schena, E.; Azhari, H.; Saccomandi, P.; Weitz, I. S., Laser-induced thermal response and controlled release of copper oxide nanoparticles from multifunctional polymeric nanocarriers. *Sci Technol Adv Mater* **2021,** 22, (1), 218-233.
193. Xu, R.; Zhang, K.; Liang, J.; Gao, F.; Li, J.; Guan, F., Hyaluronic acid/polyethyleneimine nanoparticles loaded with copper ion and disulfiram for esophageal cancer. *Carbohydr Polym* **2021,** 261, 117846.
194. Wu, Z.; Zhang, P.; Wang, P.; Wang, Z.; Luo, X., Using copper sulfide nanoparticles as cross-linkers of tumor microenvironment responsive polymer micelles for cancer synergistic photo-chemotherapy. *Nanoscale* **2021,** 13, (6), 3723-3736.
195. Xiao, Z.; Zuo, W.; Chen, L.; Wu, L.; Liu, N.; Liu, J.; Jin, Q.; Zhao, Y.; Zhu, X., H2O2 Self-Supplying and GSH-Depleting Nanoplatform for Chemodynamic Therapy Synergetic Photothermal/Chemotherapy. *ACS Appl Mater Interfaces* **2021,** 13, (37), 43925-43936.
196. Cai, X.; Xie, Z.; Ding, B.; Shao, S.; Liang, S.; Pang, M.; Lin, J., Monodispersed Copper(I)-Based Nano Metal-Organic Framework as a Biodegradable Drug Carrier with Enhanced Photodynamic Therapy Efficacy. *Adv Sci (Weinh)* **2019,** 6, (15), 1900848.
197. Fang, X. L.; Akrofi, R.; Yang, H.; Chen, Q. Y., The NIR inspired nano-CuSMn(II) composites for lactate and glycolysis attenuation. *Colloids Surf B Biointerfaces* **2019,** 181, 728-733.
198. Zhang, J.; Zhao, B.; Chen, S.; Wang, Y.; Zhang, Y.; Wang, Y.; Wei, D.; Zhang, L.; Rong, G.; Weng, Y.; Hao, J.; Li, B.; Hou, X. Q.; Kang, X.; Zhao, Y.; Wang, F.; Zhao, Y.; Yu, Y.; Wu, Q. P.; Liang, X. J.; Xiao, H., Near-Infrared Light Irradiation Induced Mild Hyperthermia Enhances Glutathione Depletion and DNA Interstrand Cross-Link Formation for Efficient Chemotherapy. *ACS Nano* **2020,** 14, (11), 14831-14845.
199. Awasthi, P.; An, X.; Xiang, J.; Kalva, N.; Shen, Y.; Li, C., Facile synthesis of noncytotoxic PEGylated dendrimer encapsulated silver sulfide quantum dots for NIR-II biological imaging. *Nanoscale* **2020,** 12, (9), 5678-5684.
200. Chong, Y.; Huang, J.; Xu, X.; Yu, C.; Ning, X.; Fan, S.; Zhang, Z., Hyaluronic Acid-Modified Au–Ag Alloy Nanoparticles for Radiation/Nanozyme/Ag+ Multimodal Synergistically Enhanced Cancer Therapy. *Bioconjugate Chemistry* **2020,** 31, (7), 1756-1765.
201. Zhang, X.-S.; Xuan, Y.; Yang, X.-Q.; Cheng, K.; Zhang, R.-Y.; Li, C.; Tan, F.; Cao, Y.-C.; Song, X.-L.; An, J.; Hou, X.-L.; Zhao, Y.-D., A multifunctional targeting

probe with dual-mode imaging and photothermal therapy used in vivo. *Journal of Nanobiotechnology* **2018,** 16, (1), 42.

202. Liu, M.; Peng, Y.; Nie, Y.; Liu, P.; Hu, S.; Ding, J.; Zhou, W., Co-delivery of doxorubicin and DNAzyme using ZnO@polydopamine core-shell nanocomposites for chemo/gene/photothermal therapy. *Acta Biomater* **2020,** 110, 242-253.
203. Sun, Y.; Yan, C.; Xie, J.; Yan, D.; Hu, K.; Huang, S.; Liu, J.; Zhang, Y.; Gu, N.; Xiong, F., High-Performance Worm-like Mn-Zn Ferrite Theranostic Nanoagents and the Application on Tumor Theranostics. *ACS Appl Mater Interfaces* **2019,** 11, (33), 29536-29548.
204. Thakur, N. S.; Patel, G.; Kushwah, V.; Jain, S.; Banerjee, U. C., Facile development of biodegradable polymer-based nanotheranostics: Hydrophobic photosensitizers delivery, fluorescence imaging and photodynamic therapy. *J Photochem Photobiol B* **2019,** 193, 39-50.
205. Liu, X.; Li, B.; Fu, F.; Xu, K.; Zou, R.; Wang, Q.; Zhang, B.; Chen, Z.; Hu, J., Facile synthesis of biocompatible cysteine-coated CuS nanoparticles with high photothermal conversion efficiency for cancer therapy. *Dalton Transactions* **2014,** 43, (30), 11709-11715.
206. Moreira, A. F.; Gaspar, V. M.; Costa, E. C.; de Melo-Diogo, D.; Machado, P.; Paquete, C. M.; Correia, I. J., Preparation of end-capped pH-sensitive mesoporous silica nanocarriers for on-demand drug delivery. *European Journal of Pharmaceutics and Biopharmaceutics* **2014,** 88, (3), 1012-1025.
207. Gaspar, V. M.; Moreira, A. F.; Costa, E. C.; Queiroz, J. A.; Sousa, F.; Pichon, C.; Correia, I. J., Gas-generating TPGS-PLGA microspheres loaded with nanoparticles (NIMPS) for co-delivery of minicircle DNA and anti-tumoral drugs. *Colloids and Surfaces B: Biointerfaces* **2015,** 134, 287-294.
208. Bernd, A.; Ott, M.; Ishikawa, H.; Schroten, H.; Schwerk, C.; Fricker, G., Characterization of efflux transport proteins of the human choroid plexus papilloma cell line HIBCPP, a functional in vitro model of the blood-cerebrospinal fluid barrier. *Pharmaceutical research* **2015,** 32, (9), 2973-82.
209. Huang, M.-H.; Yang, M.-C., Swelling and biocompatibility of sodium alginate/poly(γ-glutamic acid) hydrogels. *Polymers for Advanced Technologies* **2010,** 21, (8), 561-567.
210. Spedalieri, C.; Szekeres, G. P.; Werner, S.; Guttmann, P.; Kneipp, J., Intracellular optical probing with gold nanostars. *Nanoscale* **2021,** 13, (2), 968-979.

211. Hotze, E. M.; Phenrat, T.; Lowry, G. V., Nanoparticle Aggregation: Challenges to Understanding Transport and Reactivity in the Environment. *Journal of Environmental Quality* **2010,** 39, (6), 1909-1924.
212. Tian, F.; Conde, J.; Bao, C.; Chen, Y.; Curtin, J.; Cui, D., Gold nanostars for efficient in vitro and in vivo real-time SERS detection and drug delivery via plasmonic-tunable Raman/FTIR imaging. *Biomaterials* **2016,** 106, 87-97.
213. Li, Z.; Yang, F.; Wu, D.; Liu, Y.; Gao, Y.; Lian, H.; Zhang, H.; Yin, Z.; Wu, A.; Zeng, L., Ce6-Conjugated and polydopamine-coated gold nanostars with enhanced photoacoustic imaging and photothermal/photodynamic therapy to inhibit lung metastasis of breast cancer. *Nanoscale* **2020,** 12, (43), 22173-22184.
214. Li, D.; Zhang, Y.; Wen, S.; Song, Y.; Tang, Y.; Zhu, X.; Shen, M.; Mignani, S.; Majoral, J.-P.; Zhao, Q.; Shi, X., Construction of polydopamine-coated gold nanostars for CT imaging and enhanced photothermal therapy of tumors: an innovative theranostic strategy. *Journal of Materials Chemistry B* **2016,** 4, (23), 4216-4226.
215. Song, C.; Li, F.; Guo, X.; Chen, W.; Dong, C.; Zhang, J.; Zhang, J.; Wang, L., Gold nanostars for cancer cell-targeted SERS-imaging and NIR light-triggered plasmonic photothermal therapy (PPTT) in the first and second biological windows. *Journal of Materials Chemistry B* **2019,** 7, (12), 2001-2008.
216. Espinosa, A.; Silva, A. K. A.; Sánchez-Iglesias, A.; Grzelczak, M.; Péchoux, C.; Desboeufs, K.; Liz-Marzán, L. M.; Wilhelm, C., Cancer Cell Internalization of Gold Nanostars Impacts Their Photothermal Efficiency In Vitro and In Vivo: Toward a Plasmonic Thermal Fingerprint in Tumoral Environment. *Advanced Healthcare Materials* **2016,** 5, (9), 1040-1048.
217. Cenni, E.; Ciapetti, G.; Stea, S.; Corradini, A.; Carozzi, F., Biocompatibility and performance in vitro of a hemostatic gelatin sponge. *Journal of biomaterials science. Polymer edition* **2000,** 11, (7), 685-99.